POLITECNICO DI TORINO
Repository ISTITUZIONALE

Arbitrarily Oriented Perfectly Conducting Wedge over a Dielectric Half-Space: Diffraction and Total Far Field

Original
Arbitrarily Oriented Perfectly Conducting Wedge over a Dielectric Half-Space: Diffraction and Total Far Field / Daniele, Vito; Lombardi, Guido. - In: IEEE TRANSACTIONS ON ANTENNAS AND PROPAGATION. - ISSN 0018-926X. - STAMPA. - 64:4(2016), pp. 1416-1433. [10.1109/TAP.2016.2524412]

Availability:
This version is available at: 11583/2645379 since: 2016-07-20T18:41:54Z

Publisher:
Institute of Electrical and Electronics Engineers Inc.

Published
DOI:10.1109/TAP.2016.2524412

Terms of use:
openAccess

This article is made available under terms and conditions as specified in the corresponding bibliographic description in the repository

Publisher copyright
IEEE postprint/Author's Accepted Manuscript

©2016 IEEE. Personal use of this material is permitted. Permission from IEEE must be obtained for all other uses, in any current or future media, including reprinting/republishing this material for advertising or promotional purposes, creating new collecting works, for resale or lists, or reuse of any copyrighted component of this work in other works.

(Article begins on next page)

05 May 2023

Arbitrarily Oriented Perfectly Conducting Wedge over a Dielectric Half-Space: Diffraction and Total Far Field

Vito Daniele, and Guido Lombardi, *Senior Member, IEEE*

***Abstract*—Complex scattering targets are often made by structures constituted by wedges and penetrable substrates which may interact at near field. In this paper we describe a complete procedure to study this problem with possible developments in radar technologies (like GPR), antenna development or electromagnetic compatibility (tips near substrates). The diffraction of an incident plane wave by a perfectly conducting wedge over a dielectric half-space is studied using generalized Wiener-Hopf equations, and the solution is obtained using analytical and numerical-analytical approaches that reduce the Wiener-Hopf factorization to integral equations. The mathematical aspects are described in a unified and consistent theory for angular and layered region problems. The proposed procedure is valid for the general case and the paper focuses on E-polarization at normal incidence. The solutions are given in terms of GTD/UTD diffraction coefficients and total far fields for engineering applications. The paper presents several numerical test cases that show the validity of the proposed methods.**

***Index Terms*—Wedges, Isotropic media, Dielectric substrate, Wiener-Hopf method, Integral equations, Analytical-numerical methods, Geometrical optics, Electromagnetic diffraction, Geometrical and Uniform theory of diffraction, Near-field interactions, Radar applications, Electromagnetic Compatibility.**

I. Introduction

ACCURATE and efficient solutions to diffraction problems are of great interest in electromagnetic engineering communities, in particular when studying complex structures made of composite materials with near-field interactions. For example, in radar technologies (like GPR), antenna development or electromagnetic compatibility, complex structures may be constituted by wedges near penetrable substrates.

This paper considers the problem constituted by the evaluation of the electromagnetic field scattered by an arbitrarily oriented perfectly conducting (PEC) wedge over a dielectric half-space at a distance d, Fig.1. Cartesian coordinates (x, y) as well as polar coordinates (ρ, φ) will be used to describe the problem. The wedge structure is delimited by the PEC face a at $\varphi = \Phi_a$ and the PEC face b at $\varphi = -\pi - \Phi_b$, and it is illuminated by a plane wave. The domain of the problem is subdivided into three regions: the angular region 1 $(0 \leq \varphi < \Phi_a)$, the layered region 2 $(y \leq 0)$, the angular region 3 $(-\pi - \Phi_b < \varphi \leq -\pi)$. Regions 1 and 3 are filled with a low-dense lossless isotropic homogeneous dielectric medium, which, without loss of completeness, can be considered free space with permittivity ε_o, permeability μ_o and propagation constant $k = \omega\sqrt{\mu_o\,\varepsilon_o}$. Region 2 is constituted by a finite layer $(-d < y \leq 0)$ and a high-dense lossless isotropic homogeneous dielectric half-space $(y < -d)$. The finite layer is homogenous to regions 1 and 3, while the infinite dielectric medium is characterized by a real relative permittivity ε_r and without loss of generality by a relative permeability $\mu_r = 1$ $(k_1 = \omega\sqrt{\mu_o\varepsilon_r\varepsilon_o})$ and it is at a distance d from the edge of the wedge that can even be zero (contact between edge and dielectric). For the sake of simplicity, the incident plane wave will be assumed E_z-polarized with direction $\varphi = \varphi_o$ $(0 \leq \varphi_o < \Phi_a)$. The general skew incidence case does not introduce conceptual difficulties but doubles the number of equations to be solved.

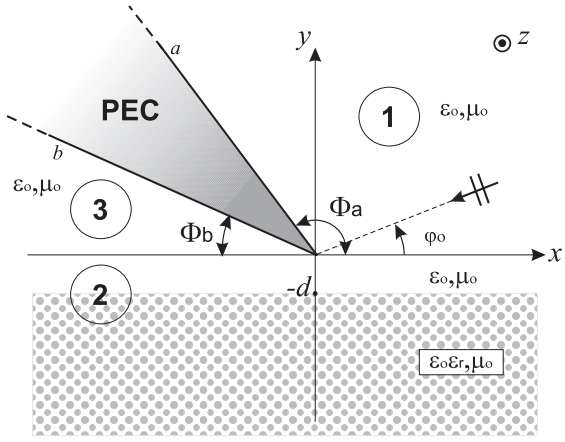

Fig. 1. The arbitrarily oriented PEC wedge over a dielectric half-space.

To our knowledge, the scientific literature does not contain solutions for the proposed problem in the spectral domain. However, the problem considered in this paper is close to several topics of great interest that have been studied by many authors. A related topic is diffraction by a buried body. Particular cases of a wedge immersed in a lossy medium were studied in [1],[2] by using the Uniform Theory of Diffraction (UTD) with limitation when the wedge is near the interface between the two media. Solutions for the scattering by a conducting strip over a lossy half-space are reported in [3],[4]. The physical optics expression for the RCS of a PEC flat plate over a dielectric half-space is described in [5]. Moreover, a lot of effort has been made in the field of integral equations (IEs) methodology by computing the Green function for layered

Manuscript received —; revised —.

The authors are with DET, Politecnico di Torino, Corso Duca degli Abruzzi 24, 10129 Torino, Italy (emails: vito.daniele@polito.it, guido.lombardi@polito.it, fax: +39-011-5644099).

Vito Daniele is also with Istituto Superiore Mario Boella (ISMB), Torino, Italy, (web: http://www.ismb.it/).

media, for instance see [6], [7]. Stemming from these works, a lot of literature has focused on scattering by buried PEC structures with IEs formulation in the spatial domain, see [8]-[10] and references therein. We recall that the use of finite methods should be combined with suitable singular basis functions capable of modeling the singularity of the physical quantities [11],[12].

Recently, the authors of this paper have shown that the Generalized Wiener-Hopf (GWH) method is a novel and effective technique to solve electromagnetic problems involving isolated impenetrable and penetrable wedges [13]-[23], in particular with the solution of the GWH problem via the approximate solution of Fredholm integral equations (FIEs) [15], [24]-[26]. In the authors' opinion, the GWH technique completes the spectral techniques developed in the past to study angular regions such as the Sommerfeld-Malyuzhinets technique (see [28]-[31] and reference therein) and the methods based on the Kontorovich-Lebedev transform (see [32]-[34] and reference therein).

The aim of this paper is to successfully apply the GWH method to numerically solve the problem considered in Fig. 1, by using a unique entire model that takes into account the true near-field interaction of the PEC wedge with the dielectric half-space to obtain precise field estimation. In particular the Wiener-Hopf (WH) technique is extended to simultaneously deal with problems where angular regions and rectangular regions coexist. In preliminary works [35]-[36] a simplified version of the problem when face b is parallel to the interface ($\Phi_b = 0$) and the angular region 1 is obtuse ($\Phi_a > \varphi_o > \pi/2$) has been analyzed in terms of free space GTD coefficients. The extension to the general case of the arbitrary orientation of faces a and b is not trivial [37]-[38] and it requires some effort, particularly in the presence of acute angular regions. Moreover, a deep study of the field inside the dielectric region requires the correct evaluation of the spectra of the electromagnetic fields near the branch points originated by the spectral propagation constants due to the presence of different media. In this paper, uniform formulas are given in order to calculate the field strength and phase for any direction in each region.

The GWH formulation of the problem is described in Sections II.A and II.B, respectively, for the angular regions, see (5)-(6), and the layered dielectric region, see (12)-(13), where we define the WH unknowns in terms of Laplace/Fourier transformations of the field components. Sections III.A and III.B present valid FIEs in each region in the spectral domain and in the angular complex plane w (typically used in Sommerfeld integrals for GTD computation). Finally a consistent and solvable system of FIEs is given in Section III.C (52)-(53). Since the numerical solution of the system provides approximate representations of an analytical element of the WH unknowns in the angular complex plane w, Appendix A is devoted to how to analytically extend the solution via difference equations. Section IV deals with the evaluation of the electromagnetic far field in the whole spatial domain for E_z-polarization in terms of Geometrical Optics (GO) components and uniform diffracted components (UTD). Finally, numerous significant test cases are presented in Section V to validate our technique and practical discussions are included with physical interpretation. The results show the convergence, the efficiency and the efficacy of the proposed method by calculating the approximated spectra of the field components. A comparison with the exact solution is only possible in the free space limit ($\varepsilon_r = 1$). The approximated spectra allow, in particular, to compute diffraction diagrams and total far field.

For the sake of clarity, we summarize the mathematical procedure by the following steps:

- Generalized Wiener-Hopf equations (Sec. II)
- Fredholm integral equations in w plane and their discretization (Sec. III)
- Analytical extension (Appendix A)
- Asymptotic solution and Total Far Field (Sec. IV)

II. The generalized Wiener-Hopf formulation

With reference to Fig. 1, Section I describes the geometry and the material properties of the problem, which is studied by considering time harmonic electromagnetic fields with a time dependence specified by the factor $e^{j\omega t}$ which is omitted. In order to facilitate the extrapolation of the equations and mathematical properties from region 1 to region 3, we introduce the supplementary angular coordinate defined by ($\overline{\varphi} = -\pi - \varphi$). Thus, the angular region 3 is also defined by ($0 \leq \bar{\varphi} < \Phi_b$). The source is an incident E_z-polarized plane wave having the following longitudinal component:

$$E_z^i = E_o e^{jk\,\rho\cos(\varphi-\varphi_o)} \tag{1}$$

where φ_o is the azimuthal angle which defines the direction of the plane wave and $k = \omega\sqrt{\mu_o\,\varepsilon_o}$ is the propagation constant of region 1. Without loss of generality, we suppose that the remote source originates from region 1, thus $0 < \varphi_o < \Phi_a$. To derive the formulation of the problem in the spectral domain we define the following Laplace/Fourier transforms:

$$\begin{cases} V_+(\alpha,\varphi) = \int_0^\infty E_z(\rho,\varphi)e^{j\alpha\,\rho}d\rho \\ I_+(\alpha,\varphi) = \int_0^\infty H_\rho(\rho,\varphi)e^{j\alpha\,\rho}d\rho \end{cases}, \quad (y \geq 0) \tag{2}$$

$$\begin{cases} v(\eta,y) = \int_{-\infty}^\infty E_z(x,y)e^{j\eta\,x}dx \\ i(\eta,y) = \int_{-\infty}^\infty H_x(x,y)e^{j\eta\,x}dx \end{cases}, \quad (y \leq 0) \tag{3}$$

To determine the GWHEs we will make extensive reference to the following quantities labeled axial spectral unknowns:

$$\begin{array}{l} V_+(\eta) = V_+(\alpha=\eta,0),\ I_+(\eta) = I_+(\alpha=\eta,0), \\ V_{\pi+}(\eta) = V_+(\alpha=\eta,-\pi),\ I_{\pi+}(\eta) = I_+(\alpha=\eta,-\pi), \\ V_-(\eta) = V_{\pi+}(-\eta),\ I_-(\eta) = -I_{\pi+}(-\eta). \end{array} \tag{4}$$

These quantities are labeled with $\pm$ subscripts: $+$ indicates plus functions in the complex plane η, *i.e.* functions that converge in an upper half-plane ($Im[\eta] > Im[\eta_{up}]$); conversely $-$ indicates minus functions that converge in a lower half-plane ($Im[\eta] < Im[\eta_{lo}]$). The $+$ ($-$) functions are considered non-conventional if $Im[\eta_{up}] > 0$ ($Im[\eta_{lo}] < 0$). The axial spectral unknowns are Laplace transforms evaluated in $\varphi = 0, \pm\pi$ directions. Without loss of generality, to avoid the presence of singularities on the real axis of the η plane, the propagation constants k and k_1 are assumed with a negative (vanishing) imaginary part also in the presence of lossless media.

A. Angular regions

According to the theory presented in [14]-[17], the GWHEs for the angular regions 1 and 3 are respectively

$$Y_c(\eta)\, V_+(\eta) - I_+(\eta) = -I_{a+}(-m_a(\eta)) \tag{5}$$

$$Y_c(\eta)\, V_{\pi+}(\eta) + I_{\pi+}(\eta) = I_{b+}(-m_b(\eta)) \tag{6}$$

where

$$I_{a+}(-m_a) = \int_0^\infty H_\rho(\rho,\Phi_a)e^{-jm_a\rho}d\rho \tag{7}$$

$$I_{b+}(-m_b) = \int_0^\infty H_\rho(\rho,-\pi-\Phi_b)e^{-jm_b\rho}d\rho \tag{8}$$

are unknowns respectively defined on face a and b in terms of spectral variables $m_{a,b}(\eta) = -\eta\cos\Phi_{a,b} + \xi(\eta)\sin\Phi_{a,b}$, free-space spectral admittance $Y_c(\eta) = \frac{1}{Z_c(\eta)} = \frac{\xi(\eta)}{kZ_o}$, free-space spectral propagation constant $\xi(\eta) = \sqrt{k^2-\eta^2}$ (with $\xi(0)=k$) and free space impedance $Z_o = 1/Y_o$.

B. Layered region

According to the theory of layered regions, which use transmission line modeling, see for example [26] and [27], the following spectral impedance relation holds for region 2:

$$Y(\eta)v(\eta,0) = -i(\eta,0) \tag{9}$$

The admittance $Y(\eta) = 1/Z(\eta)$ is the one seen at $y=0$

$$Y(\eta) = \frac{Y_d(\eta)\cos(\xi(\eta)d) + jY_c(\eta)\sin(\xi(\eta)d)}{Y_c(\eta)\cos(\xi(\eta)d) + jY_d(\eta)\sin(\xi(\eta)d)}Y_c(\eta) \tag{10}$$

where $Y_d(\eta) = \frac{1}{Z_d(\eta)} = -\frac{i(\eta,-d)}{v(\eta,-d)} = \frac{\xi_d(\eta)}{k\,Z_o}$ is the spectral admittance of the dielectric region and $\xi_d(\eta) = \sqrt{\varepsilon_r k^2-\eta^2}$ is the spectral propagation constant. From (2), (3) and (4)

$$\begin{array}{l} v(\eta,0) = V_{\pi+}(-\eta) + V_+(\eta), \\ i(\eta,0) = -I_{\pi+}(-\eta) + I_+(\eta), \end{array} \tag{11}$$

thus we obtain the following Wiener-Hopf equation (WHE)

$$Y(\eta)(V_{\pi+}(-\eta) + V_+(\eta)) - I_{\pi+}(-\eta) + I_+(\eta) = 0 \tag{12}$$

Substituting $\eta \to -\eta$ in (12) we obtain an independent WHE

$$Y(-\eta)(V_{\pi+}(\eta) + V_+(-\eta)) - I_{\pi+}(\eta) + I_+(-\eta) = 0 \tag{13}$$

Moreover, according to the transmission line theory we have

$$v(\eta,y) = \frac{Z_d\cos\left(\xi\,(d+y)\right) + jZ_c\sin\left(\xi\,(d+y)\right)}{Z_d\cos(\xi\,d) + jZ_c\sin(\xi\,d)}v_\eta(0),\ -d\le y\le 0 \tag{14}$$

with Z_d, Z_c and ξ functions of η; and for $y<-d$

$$v(\eta,y) = v_\eta(\eta,-d)e^{j\xi_d(y+d)},\ y<-d \tag{15}$$

with $\xi_d = \xi_d(\eta)$. The reflection coefficients for the incident wave respectively at $y=-d$ and $y=0$ are

$$\Gamma_{RD} = \frac{Y_c(\eta_o) - Y_d(\eta_o)}{Y_c(\eta_o) + Y_d(\eta_o)},\ \Gamma_o = \frac{Y_c(\eta_o) - Y(\eta_o)}{Y_c(\eta_o) + Y(\eta_o)} \tag{16}$$

The system of GWHEs (5), (6), (12), (13) can be exactly solved in closed form only when the dielectric half-space is not present, *i.e.* when the PEC wedge is immersed in free space. Since exact solutions for the general case are not available, we resort to approximate numerical-analytical methods based on Fredholm integral equations (FIEs) to obtain approximate factorizations [15], [24]-[26].

III. Fredholm integral equations for factorization in w-plane

The system of four GWHEs (5), (6), (12), (13) are defined into four complex planes $(\eta,-\eta,m_a,m_b)$ with six unknowns $V_+(\cdot), I_+(\cdot), V_{\pi+}(\cdot), I_{\pi+}(\cdot), I_{a+}(\cdot), I_{b+}(\cdot)$. In order to obtain an approximate solution, we resort to approximate factorization by reducing (5), (6), (12), (13) to FIEs where the unknowns $I_{a+}(-m_a(\eta))$, $I_{b+}(-m_b(\eta))$, $I_{\pi+}(-\eta)$, $I_+(-\eta)$ do not appear [36], since they are eliminated through decomposition. Since (5), (6) for regions 1 and 3 are cumbersome to be decomposed in η-plane especially for acute aperture angles $(0<\Phi_{a,b}<\pi/2)$, we introduce the angular complex plane w

$$\eta = -k\cos(w) \tag{17}$$

already successfully applied in angular region problems [14], [16], [18], [22], [23], see Section III.A. The mapping between η and w has been studied extensively in [14], Appendix I of [18] and [26] and, it presents several important properties. In particular we recall that, by using the notation $F(-k\cos w) = \hat{F}(w)$, the plus functions in η are even functions of w [14].

In order to make a consistent system of equations also (12), (13) of region 2 will be formulate in terms of FIEs in the angular complex plane w, see Section III.B.

In Section III.C the resulting system of four FIEs with unknowns $\hat{V}_+(w), \hat{I}_+(w), \hat{V}_{\pi+}(w), \hat{I}_{\pi+}(w)$, *i.e.* the axial spectra in the angular complex plane w, is reduced to two coupled FIEs (52)-(53) with unknowns $\hat{V}_+(w), \hat{V}_{\pi+}(w)$ that is numerically solved.

A. FIEs for Angular regions

In [36] FIEs are obtained with a lot of mathematical effort in η-plane for obtuse angles. To deal with the general case we resort to the angular complex plane w.

Let's first consider the angular region 1. Taking into account that $m_a = +k\cos(w+\Phi_a)$, in the w-plane (5) becomes

$$-Y_o\hat{V}_d(w) - \hat{I}_+(w) = -\hat{I}_{a+}(w+\Phi_a) \tag{18}$$

or equivalently

$$Y_o\hat{V}_d(w-\Phi_a) + \hat{I}_+(w-\Phi_a) = \hat{I}_{a+}(w) \tag{19}$$

where $\hat{V}_d(w) = \sin w\hat{V}_+(w)$, $\hat{Y}_c(w) = -Y_o\sin(w)$ $(\xi(w) = -k\sin(w))$, thus $\hat{Y}_c(w)\hat{V}_+(w) = -Y_o\hat{V}_d(w)$. Substituting $w\to -w$ and using $\hat{I}_{a+}(w) = \hat{I}_{a+}(-w)$ we obtain

$$\hat{I}_+(w+\Phi_a) - \hat{I}_+(w-\Phi_a) = Y_o\left[\hat{V}_d(w+\Phi_a) + \hat{V}_d(w-\Phi_a)\right] \tag{20}$$

that is a difference equation in the w-plane that relates $\hat{I}_+(w)$ to $\hat{V}_d(w)$. In order to obtain $\hat{I}_+(w)$ as a function of $\hat{V}_d(w)$ (Norton representation) we apply the Malyuzhinets-Fourier (M-F) transform[1] [39]. According to the Malyuzhinets theory (see also [39]) the scattered field (the total field minus the incident field) is regular in the strip $-\Phi_a \le \mathrm{Re}[w] \le \Phi_a$, thus $\hat{V}_d(w)$ and $\hat{I}_+(w)$ are regular in $-\Phi_a \le \mathrm{Re}[w] \le \Phi_a$ except

[1]The Malyuzhinets-Fourier (M-F) transform

$\bar{F}[t] = \mathcal{MF}\{\hat{F}(w)\} = -j\int_{-j\infty}^{j\infty}\hat{F}(w)\mathrm{e}^{+jtw}dw, Re[t]=0$

$\hat{F}[w] = \mathcal{MF}^{-1}\{\bar{F}(t)\} = -\frac{j}{2\pi}\int_{-j\infty}^{j\infty}\bar{F}(t)\mathrm{e}^{-jtw}dt, Re[w]=0$

for the poles $\pm\varphi_o$ due to the incident field. With this consideration, by using the transport theorem and the convolution theorem in M-F in (20), we obtain a pure algebraic equation in M-F domain (t plane), whose M-F inverse transformation gives the following generalized Norton representation (21) in terms of $\hat{I}_+(w)$ and $\hat{V}_d(w)$ for $Re[w]=0$ which is a singular integral representation [35]:

$$\hat{I}_+(w) = j\frac{Y_o}{2\Phi_a}\mathcal{P}.\mathcal{V}.\int_{-j\infty}^{j\infty}\cot(\frac{\pi}{2\Phi_a}(w-w'))\hat{V}_d(w')dw' + \hat{I}_N(w) \tag{21}$$

where $\hat{I}_N(w) = j\frac{\pi Y_o}{k\Phi_a}\frac{2\sin(\frac{\pi}{\Phi_a}\varphi_o)}{\cos(\frac{\pi}{\Phi_a}w)-\cos(\frac{\pi}{\Phi_a}\varphi_o)}$ and $\mathcal{P}.\mathcal{V}.$ denotes the principal value.

The singular integral representation (21) is equivalent to

$$\hat{I}_+(w) = -Y_o\hat{V}_d(w) + \frac{jY_o}{2\Phi_a}\int_M \cot\left(\frac{\pi}{2\Phi_a}(w-w')\right)\hat{V}_d(w')dw' + \hat{I}_N(w) \tag{22}$$

for $Re[w]<0$ where the integration line is the imaginary axis M ($Re[w']=0$). In order to obtain good numerical convergence in the angular complex plane w, we have successfully experienced the application of the contour deformation that warps M into M_1 ($Re[w']=-\pi/2$). However in (22) we need to take into account the structural poles of the kernel $w'=\pm(w+2n\Phi_a)$, $n\in\mathbb{Z}$, that arise from the poles of $\cot(\cdot)$ in the integral kernel. In wedge problems treated with GWHEs we have successfully applied the mapping

$$w_a = \frac{\pi}{\Phi_a}w \tag{23}$$

which allows good properties of convergence by warping M_a ($Re[w_a']=0$) into M_{a1} ($Re[w_a']=-\pi/2$, *i.e.* $Re[w']=-\Phi_a/2$). This deformation avoids the interaction with structural poles also for acute angular regions (this property is not true in the w plane and in the η plane). This result justifies the validity of [23] where the concave wedge with anisotropic surface impedance is studied in w_a plane.

Using symmetry of trigonometric functions and (23) in (22)

$$\frac{\pi}{\Phi_a}\int_{-j\infty}^{j\infty}\cot\left(\frac{\pi}{2\Phi_a}(w-w')\right)\hat{V}_d(w')dw' = \int_{M_a}\frac{\sin w_a{}'}{\cos w_a{}' - \cos w_a}\tilde{V}_d(w_a{}')dw_a \tag{24}$$

for $Re[w_a]<0$ where $\tilde{V}_d(w_a)=\hat{V}_d(\frac{\Phi_a}{\pi}w)$. Taking into account the properties of regularity of the integral kernel and of $\tilde{V}_d(w_a)$, the warping of M_a into M_{a1} may capture only the pole singularity $w_{ao}=-\frac{\pi}{\Phi_a}\varphi_o$ due to the incident field if $0<\varphi_o<\Phi_a/2$ (we recall that $\tilde{V}_d(w_a)-\tilde{V}_d^i(w_a)$ is regular in the strip $-\pi<\mathrm{Re}[w_a{}']<\pi$). Since

$$\mathrm{Res}[\tilde{V}_d^i(w_a)]\Big|_{w_a=w_{ao}} = \frac{\pi}{\Phi_a}\frac{j}{k}E_o \tag{25}$$

we obtain that (24) is equivalent to

$$\int_{M_{a1}}\frac{\sin w_a{}'}{\cos w_a{}' - \cos w_a}\tilde{V}_d(w_a{}')dw_a + \frac{2\pi^2 E_o}{\Phi_a k}\frac{\sin\frac{\pi}{\Phi_a}\varphi_o u(\frac{\Phi_a}{2}-\varphi_o)}{\cos\frac{\pi}{\Phi_a}\varphi_o - \cos w_a} \tag{26}$$

where $u(\delta)$ is the unit step function. By using (24) with (26) in (22), we obtain a new form of the singular integral representation with integration line M_{a1} that is valid for $Re[w_a]<-\pi/2$ since its integral kernel

$$K(w_a, w_a') = \frac{\sin w_a{}'}{\cos w_a' - \cos w_a} \tag{27}$$

is singular. In order to obtain a non singular kernel $K_m(w_a,w_a')$ we modify $K(w_a,w_a')$ by adding

$$K_1(w_a,w_a') = -\frac{\Phi_a}{\pi}\frac{\sin\frac{\Phi_a}{\pi}w_a}{\cos\frac{\Phi_a}{\pi}w_a' - \cos\frac{\Phi_a}{\pi}w_a} \tag{28}$$

to $K(w_a,w_a')$ with the following properties:

1) $Res[(K(w_a,w_a')+K_1(w_a,w_a'))\tilde{V}_d(w_a')]\Big|_{w_a=w_a'} = 0$
2) $\int_{M_a}K_1(w_a,w_a')\tilde{V}_d(w_a{}')dw_a = 0 =$
$= \int_{M_{a_1}}K_1(w_a,w_a')\tilde{V}_d(w_a{}')dw_a - \frac{2\pi E_o}{k}\frac{(\sin w)u(\frac{\Phi_a}{2}-\varphi_o)}{\cos\varphi_o-\cos w}$

While property 1) makes the new kernel (29) not singular and compact, property 2) shows how $K_1(w_a,w_a')$ does not change the mathematical property of the integral equation. The second property shows also how the integral changes when the warping of M_a into M_{a1} is applied taking into account the possibility of capturing the pole singularity $w_{ao}=-\frac{\pi}{\Phi_a}\varphi_o$ via (25). It yields

$$K_m(w_a,w_a') = (K(w_a,w_a')+K_1(w_a,w_a')) \tag{29}$$

As a final result we obtain (30), *i.e.* the FIE for region 1, whose kernel is compact, thus the constraint $Re[w_a]<-\pi/2$ is not necessary anymore:

$$\hat{I}_+(w) = -Y_o\hat{V}_d(w) + \frac{jY_o}{2\pi}\int_{M_{a1}}K_m(w_a,w_a{}')\tilde{V}_d(w_a{}')dw_a{}' + \hat{I}_{NC}(w) \tag{30}$$

where

$$\hat{I}_{NC}(w) = +\frac{j\pi Y_o E_o}{k\Phi_a}\frac{2\sin(\frac{\pi}{\Phi_a}\varphi_o)}{\cos(w_a)-\cos(\frac{\pi}{\Phi_a}\varphi_o)} + -\frac{j\pi Y_o E_o}{k\Phi_a}\frac{\sin(\frac{\pi}{\Phi_a}\varphi_o)u(\frac{\Phi_a}{2}-\varphi_o)}{\cos(w_a)-\cos(\frac{\pi}{\Phi_a}\varphi_o)} - j\frac{Y_o E_o}{k}\frac{(\sin w)\,u(\frac{\Phi_a}{2}-\varphi_o)}{\cos w-\cos\varphi_o} \tag{31}$$

Using the same reasoning, in region 3, from (6) we obtain in the w-plane ($m_b=+k\cos(w+\Phi_b)$)

$$-Y_o\hat{V}_{\pi d}(w-\Phi_b)+\hat{I}_{\pi+}(w-\Phi_b) = -Y_o\hat{V}_{\pi d}(w+\Phi_b)-\hat{I}_{\pi+}(w+\Phi_b) \tag{32}$$

where $\hat{V}_{\pi d}(w)=\sin w\hat{V}_{\pi+}(w)$. It yields the following FIE

$$\hat{I}_{\pi+}(w) = Y_o\hat{V}_{\pi d}(w) + -\frac{jY_o}{2\pi}\int_{M_{b1}}[\frac{\sin w_b{}'}{\cos w_b'-\cos w_b} - \frac{\frac{\Phi_b}{\pi}\sin\frac{\Phi_b}{\pi}w_b}{\cos\frac{\Phi_b}{\pi}w_b'-\cos w}]\,\tilde{V}_{\pi d}(w_b')dw_b' \tag{33}$$

where $\tilde{V}_d(w_b)=\hat{V}_d(\frac{\Phi_b}{\pi}w)$ with $w_b=\frac{\pi}{\Phi_b}w$.

Eqs. (30) and (33) are FIEs that hold respectively in region 1 and in region 3. The main difference between the two equations is that (33) does not have source term. This is due to the fact that no plane wave with infinite support is present in region 3, in particular along negative x axis. On the contrary in region 1 the incident field is taken into account since its support is infinite along positive x axis.

An important property of (30) and (33) is that their integral parts do not present the pole singularities of the unknowns thus their contributions are correction terms to the GO field.

B. FIEs for the layered region

While the WH equations contain plus and minus unknowns, their integral representations presents just one kind of unknowns (plus or minus). In general, the reduction of the WH equations to integral representations is obtained by decomposition through Cauchy integration and it requires the evaluation of the not conventional part of the unknowns with extraction of offending singularities. The non conventional part of a plus (minus) function is defined by the part that presents singularities in the standard regularity half plane $Im[\eta] \geq 0$ ($Im[\eta] \leq 0$). Generally the non conventional singularities are poles arising from geometrical optics (GO) contributions that diverge on the line of integration of the transformation of the unknowns. Taking into account (1)-(4), the GO contributions yield the pole $\eta_o = -k\cos\varphi_o$ in the spectra of the axial unknowns $V_+(\eta)$ and $I_+(\eta)$. This pole is not conventional for plus functions if $\varphi_o < \pi/2$. Consequently the non conventional parts of $V_+(\eta)$ and $I_+(\eta)$ are respectively:

$$S_{v_+}(\eta) = \frac{R_v}{\eta-\eta_o}u(\frac{\pi}{2}-\varphi_o),\ S_{i_+}(\eta) = \frac{R_i}{\eta-\eta_o}u(\frac{\pi}{2}-\varphi_o) \quad (34)$$

where R_v and R_i are related to the GO field composed of the incident plane wave and the plane wave reflected by the dielectric half-space resulting at $y = 0$:

$$R_v = j(1+\Gamma_o)E_o,\ R_i = -j(1-\Gamma_o)\frac{E_o}{Z_o}\sin(\varphi_o) \quad (35)$$

where Γ_o is defined in (16).

Concerning the unknowns $V_{\pi+}(\eta)$ and $I_{\pi+}(\eta)$, simple ray tracing considerations show that the GO contribution is present only on a finite segment of the negative x axis. Thus, since $V_{\pi+}(\eta)$ and $I_{\pi+}(\eta)$ are Laplace transforms of functions, it yields that $V_{\pi+}(\eta)$ and $I_{\pi+}(\eta)$ do not show poles and consequently are always conventional.

The procedure to deduce integral representations of the GWHEs (12) and (13) is based on the elimination of the minus unknowns $\hat{I}_{\pi+}(-\eta)$ and $\hat{I}_+(-\eta)$ through Cauchy integrals (36) that decompose a given function as a sum of conventional minus $F_-(\eta)$ and plus functions $F_+(\eta)$ [15],[25],[26]:

$$F_+(\eta) = \frac{1}{2\pi j}\int_{\gamma_{1\eta}}\frac{F(\eta')}{\eta'-\eta}d\eta',\ F_-(\eta) = -\frac{1}{2\pi j}\int_{\gamma_{2\eta}}\frac{F(\eta')}{\eta'-\eta}d\eta' \quad (36)$$

where the two integration paths $\gamma_{1\eta}$ and $\gamma_{2\eta}$ are called respectively the *smile* real axis and the *frown* real axis, see [25], [26]. These integration paths are the deformed real axis that pass respectively below and above the pole $\eta' = \eta$.

The procedure starts by using (12) in the form

$$-I_{\pi+}(-\eta) = -Y(\eta)(V_{\pi+}(-\eta)+V_+(\eta)) - I_+(\eta) \quad (37)$$

To get the FIE related to (37) we use several intermediate steps based on contour integration of the unknowns. Since $I_-(\eta) = -I_{\pi+}(-\eta)$ is a conventional function we obtain that its contour integration along $\gamma_{1\eta}$ is null, $\frac{1}{2\pi j}\int_{\gamma_{1\eta}}\frac{I_-(\eta')}{\eta'-\eta}d\eta' = 0$, thus from (37) it yields

$$\frac{1}{2\pi j}\int_{\gamma_{1\eta}}\frac{-Y(\eta')(V_{\pi+}(-\eta')+V_+(\eta'))-I_+(\eta')}{\eta'-\eta}d\eta' = 0 \quad (38)$$

Since $\frac{1}{2\pi j}\int_{\gamma_{1\eta}}\frac{V_{\pi+}(-\eta')}{\eta'-\eta}d\eta' = 0$ it yields

$$\begin{aligned}\frac{1}{2\pi j}\int_{\gamma_{1\eta}}\frac{Y(\eta')V_{\pi+}(-\eta')}{\eta'-\eta}d\eta' &= \frac{1}{2\pi j}\int_{\gamma_{1\eta}}\frac{(Y(\eta')-Y(\eta))V_{\pi+}(-\eta')}{\eta'-\eta}d\eta' = \\ &= \frac{-1}{2\pi j}\int_{-\infty}^{\infty}\frac{(Y(-\eta')-Y(\eta))V_{\pi+}(\eta')}{\eta'+\eta}d\eta'\end{aligned} \quad (39)$$

Moreover from the knowledge of the non conventional part of $V_+(\eta), I_+(\eta)$ (34) we obtain

$$\frac{1}{2\pi j}\int_{\gamma_{2\eta}}\frac{Y(\eta)\,V_+(\eta')+I_+(\eta')}{\eta'-\eta}d\eta' = -[Y(\eta)S_{v_+}(\eta)+S_{i_+}(\eta)] \quad (40)$$

The Cauchy integration in (38) and (40) yields

$$\begin{aligned}\frac{1}{2\pi j}\int_{\gamma_{1\eta}}\frac{Y(\eta')\,V_+(\eta')+I_+(\eta')}{\eta'-\eta}d\eta' &= \tfrac{1}{2}[Y(\eta)\,V_+(\eta)+I_+(\eta)]+ \\ &+\tfrac{1}{2\pi j}\mathcal{P}.\mathcal{V}.\int_{-\infty}^{\infty}\frac{Y(\eta')\,V_+(\eta')+I_+(\eta')}{\eta'-\eta}d\eta'\end{aligned} \quad (41)$$

$$\begin{aligned}\frac{1}{2\pi j}\int_{\gamma_{2\eta}}\frac{Y(\eta)\,V_+(\eta')+I_+(\eta')}{\eta'-\eta}d\eta' &= -\tfrac{1}{2}[Y(\eta)\,V_+(\eta)+I_+(\eta)]+ \\ &+\tfrac{1}{2\pi j}\mathcal{P}.\mathcal{V}.\int_{-\infty}^{\infty}\frac{Y(\eta)\,V_+(\eta')+I_+(\eta')}{\eta'-\eta}d\eta'\end{aligned} \quad (42)$$

where $\mathcal{P}.\mathcal{V}.$ denotes the principal value.

The final integral equation (43) (see the equation on top of next page) is obtained starting from (38)

1) substituting (39) into (38),
2) subtracting (40) into the resultant of step 1,
3) substituting (41) and (42) into the resultant of step 2,
4) deforming the integral path from the real axis of η ($Im[\eta] = 0$) to the imaginary axis of η ($Re[\eta] = 0$) since no source poles and branch points are in the 1st and the 3rd quadrants of the η plane,
5) applying the mapping (17) to the resultant integral equation (see Appendix I of [18] for corresponding contours in w) and by warping the imaginary axis of η into M_1 ($Re[w] = -\pi/2$).

Starting from (13) we repeat the same reasoning by eliminating $I_+(-\eta)$, yielding the integral representation (44) (see the equation on top of next page). An important property of (43) and (44) is that their integral parts do not present the pole singularities of the unknowns thus their contribution is a correction term to the GO fields. We recall that the use of w plane is necessary since for the angular regions 1 and 3 the Fredholm factorization in the η-plane is cumbersome especially to track the structural singularities. In (43) and (44) we have used the unknowns $\hat{V}_+(w)$, $\hat{V}_{\pi+}(w)$ together with $\hat{V}_d(w)$, $\hat{V}_{\pi d}(w)$, which differ for a factor $\sin w$, to make more compact the equations.

C. The system of FIEs

The system of FIEs is obtained from the two couples of equations (30),(33) and (43),(44). We note that while in (30) and (33) the integration contour path is respectively M_{a1} ($Re[w] = -\Phi_a/2$, *i.e.* $Re[w_a] = -\pi/2$) and M_{b1} ($Re[w] = -\Phi_b/2$, *i.e.* $Re[w_b] = -\pi/2$), in (43) and (44) the contour is M_1 ($Re[w] = -\pi/2$).

In order to obtain a consistent system of FIEs, we need to formulate the equations with the same integration paths

$$\hat{Y}(w)\hat{V}_{+}(w)+\hat{I}_{+}(w)+\frac{1}{2\pi j}\int_{M_1}\frac{\hat{Y}(w')-\hat{Y}(w)}{\cos w'-\cos w}\hat{V}_d(w')dw'-\frac{1}{2\pi j}\int_{M_1}\frac{\hat{Y}(w')-\hat{Y}(w)}{\cos w'+\cos w}\hat{V}_{\pi d}(w')dw'=\frac{R_i\ u(\frac{\pi}{2}-\varphi_o)}{-k\cos w+k\cos\varphi_o}+\frac{\hat{Y}(w)R_v\ u(\frac{\pi}{2}-\varphi_o)}{-k\cos w+k\cos\varphi_o} \quad (43)$$

$$\hat{Y}(w)\hat{V}_{\pi+}(w)-\hat{I}_{\pi+}(w)+\frac{1}{2\pi j}\int_{M_1}\frac{\hat{Y}(w')-\hat{Y}(w)}{\cos w'-\cos w}\hat{V}_{\pi d}(w')dw'-\frac{1}{2\pi j}\int_{M_1}\frac{\hat{Y}(w')-\hat{Y}(w)}{\cos w'+\cos w}\hat{V}_d(w')dw'=\frac{-R_i\ u(\frac{\pi}{2}-\varphi_o)}{k\cos w+k\cos\varphi_o}-\frac{\hat{Y}(w)R_v\ u(\frac{\pi}{2}-\varphi_o)}{k\cos w+k\cos\varphi_o} \quad (44)$$

and unknowns. For this reason in (43) and (44) we use w_a plane and we warp contour M_1 into M_{a1} if the integrand is $\hat{V}_d(w)$, while we use w_b plane and we warp M_1 into M_{b1} if the integrand is $\hat{V}_{\pi d}(w)$. Using (23) the contour M_1 is mapped into the contour $M_1^{(w_a)}$ *i.e.* $Re[w_a]=-\frac{\pi^2}{2\Phi_a}$, while by using using $w_b=\frac{\pi}{\Phi_b}w$ it is mapped into $M_1^{(w_b)}$ *i.e.* $Re[w_b]=-\frac{\pi^2}{2\Phi_b}$.

Starting from the first case, the contour deformation from $M_1^{(w_a)}$ into M_{a1} may capture GO poles of $\hat{V}_d(w)$: according to the Malyuzhinets theory the strip delimited by $M_1^{(w_a)}$ into M_{a1} may contain only the incident wave pole, *i.e.* $w_{ao}=-\frac{\pi}{\Phi_a}\varphi_o$, that is captured in the contour deformation when $-\frac{\pi^2}{2\Phi_a}<w_{ao}<-\frac{\pi}{2}$, that is for $\frac{\Phi_a}{2}<\varphi_o<\frac{\pi}{2}$. Other capturable singularities are the ones derived from the kernels (structural singularities) which are related to the admittance $\hat{Y}(w)$ defined by the geometrical/material parameters of the problem. In dielectric half-spaces $\hat{Y}(w)$ has branch points and structural poles.

The branch point derives from $\hat{Y}_d(w)=Y_d(-k\cos(w))=\sqrt{\varepsilon_r k^2-(-k\cos(w))^2}/(kZ_o)$, that is

$$w_{branch}=-\arccos(\pm\sqrt{\varepsilon_r}) \quad (45)$$

thus in the w_a plane $w_{a,branch}=\frac{\pi}{\Phi_a}(w_{branch}+2n\pi)$ for integer n. Following the inverse mapping described in Appendix I of [18] (also reported at (72)), if the argument of the arccos in (45) is a real positive greater than 1, $w_{a,branch}$ is on $Re[w_a]=-\frac{\pi^2}{\Phi_a}$, if negative less than -1, $w_{a,branch}$ is on $Re[w_a]=0$, *i.e.* on M_a. The structural poles are the zeros of the denominator of $\hat{Y}(w)$, *i.e.* $w=0,-\pi$. However both the branch point and the structural poles are not in the strip $-\frac{\pi^2}{2\Phi_a}<Re[w_a{}']<-\frac{\pi}{2}$ thus they do not give any contribution in the contour deformation from $M_1^{(w_a)}$ to M_{a1}.

According to the above considerations we state that

$$\int_{M_1}\frac{[\hat{Y}(w')-\hat{Y}(w)]\hat{V}_d(w')}{\cos w'-\cos w}dw'=\frac{\Phi_a}{\pi}\int_{M_1^{(w_a)}}\frac{[\tilde{Y}(w_a{}')-\hat{Y}(w)]\tilde{V}_d(w_a{}')}{\cos(\frac{\Phi_a}{\pi}w_a{}')-\cos w}dw_a{}'=$$
$$=\frac{\Phi_a}{\pi}\int_{M_{a1}}\frac{[\tilde{Y}(w_a{}')-\hat{Y}(w)]\tilde{V}_d(w_a{}')}{\cos(\frac{\Phi_a}{\pi}w_a{}')-\cos w}dw_a{}'+\frac{2\pi E_o}{k}\frac{[\hat{Y}(-\varphi_o)-\hat{Y}(w)]u_a(\varphi_o)}{\cos\varphi_o-\cos w} \quad (46)$$

where $u_a(\varphi_o)=u(\varphi_o-\Phi_a/2)-u(\varphi_o-\pi/2)$, $\tilde{V}_d(w_a)=\hat{V}_d(\frac{\Phi_a}{\pi}w)$, $\tilde{Y}(w_a)=\hat{Y}(\frac{\Phi_a}{\pi}w)$.

Similarly, the use of w_b plane and the contour deformation from $M_1^{(w_b)}$ into M_{b1} yields

$$\int_{M_1}\frac{[\hat{Y}(w')-\hat{Y}(w)]\hat{V}_{\pi d}(w')}{\cos w'+\cos w}dw'=\frac{\Phi_b}{\pi}\int_{M_1^{(w_b)}}\frac{[\tilde{Y}(w_b{}')-\hat{Y}(w)]\tilde{V}_{\pi d}(w_b{}')}{\cos(\frac{\Phi_b}{\pi}w_b{}')+\cos w}dw_b{}'=$$
$$=\frac{\Phi_b}{\pi}\int_{M_{b1}}\frac{[\tilde{Y}(w_b{}')-\hat{Y}(w)]\tilde{V}_{\pi d}(w_b{}')}{\cos(\frac{\Phi_b}{\pi}w_b{}')+\cos w}dw_b{}' \quad (47)$$

where $\tilde{V}_{\pi d}(w_b)=\hat{V}_{\pi d}(\frac{\Phi_b}{\pi}w)$, $\tilde{Y}(w_b)=\hat{Y}(\frac{\Phi_b}{\pi}w)$. We recall that no GO pole is present in the spectrum of $\hat{V}_{\pi d}(w)$.

By applying (46) and (47) to (43) and (44) we obtain the FIEs (48) and (49) for the layered region 2 that, together with the FIEs (30) and (33) for the angular regions 1 and 3, constitute a consistent and solvable system of integral equations.

The source terms of the FIEs (48) and (49) are $\hat{S}_{tot+}(w)$ and $\hat{S}_{tot\pi+}(w)$ and they are reported in explicit form respectively in (50) and (51), while the source term of (30) is $-\hat{I}_{NC}(w)$ that is reported in (31). Note that (33) is an homogenous equation.

$$\begin{aligned}\hat{S}_{tot+}(w) &= \tfrac{R_i\ u(\frac{\pi}{2}-\varphi_o)}{-k\cos w+k\cos\varphi_o}+\\ &+\tfrac{\hat{Y}(w)R_v\ u(\frac{\pi}{2}-\varphi_o)}{-k\cos w+k\cos\varphi_o}+jE_o\tfrac{[\hat{Y}(-\varphi_o)-\hat{Y}(w)]u_a(\varphi_o)}{-k\cos w+k\cos\varphi_o}\end{aligned} \quad (50)$$

$$\begin{aligned}\hat{S}_{tot\pi+}(w) &= \tfrac{-R_i\ u(\frac{\pi}{2}-\varphi_o)}{k\cos w+k\cos\varphi_o}+\\ &-\tfrac{\hat{Y}(w)R_v\ u(\frac{\pi}{2}-\varphi_o)}{k\cos w+k\cos\varphi_o}-jE_o\tfrac{[\hat{Y}(-\varphi_o)-\hat{Y}(w)]u_a(\varphi_o)}{k\cos w+k\cos\varphi_o}\end{aligned} \quad (51)$$

We recall that $u_a(\varphi_o)=u(\varphi_o-\Phi_a/2)-u(\varphi_o-\pi/2)$. The source terms of the FIEs (48),(49),(30),(33) are only composed of some of the terms in (50), (51), (31) depending on the value of φ_o and Φ_a when the incident wave impinges from region 1. The steps functions select some of the terms. We highlight three possible cases: $0<\varphi_o<\Phi_a/2$, $\pi/2<\varphi_o<\Phi_a$ and $\Phi_a/2<\varphi_o<\pi/2$.

The system of equations (48),(49),(30),(33) can be reduced to two coupled integral equations (52), (53) in terms of $\hat{V}_{+}(w)$ and $\hat{V}_{\pi+}(w)$ by eliminating $\hat{I}_{+}(w)$ and $\hat{I}_{\pi+}(w)$, where

$$\hat{G}(w)=\hat{Y}_c(w)+\hat{Y}(w)$$

$$\begin{aligned}\hat{H}_{11}(w_a,w_a{}') &= \tfrac{\Phi_a}{\pi}\tfrac{\tilde{Y}(w_a{}')-\hat{Y}(w)}{\cos(\frac{\Phi_a}{\pi}w_a{}')-\cos w}+\\ &-\tfrac{Y_o\sin w_a{}'}{\cos w_a'-\cos w_a}+\tfrac{\Phi_a}{\pi}\tfrac{Y_o\sin\frac{\Phi_a}{\pi}w_a}{\cos\frac{\Phi_a}{\pi}w_a'-\cos w}\\ \hat{H}_{12}(w_b,w_b{}') &= -\tfrac{\Phi_b}{\pi}\tfrac{\tilde{Y}(w_b{}')-\hat{Y}(w)}{\cos(\frac{\Phi_b}{\pi}w_b{}')+\cos w}\\ \hat{H}_{21}(w_a,w_a{}') &= -\tfrac{\Phi_a}{\pi}\tfrac{\tilde{Y}(w_a{}')-\hat{Y}(w)}{\cos(\frac{\Phi_a}{\pi}w_a{}')+\cos w}\\ \hat{H}_{22}(w_b,w_b{}') &= \tfrac{\Phi_b}{\pi}\tfrac{\tilde{Y}(w_b{}')-\hat{Y}(w)}{\cos(\frac{\Phi_b}{\pi}w_b{}')-\cos w}+\\ &-Y_o\tfrac{\sin w_b{}'}{\cos w_b'-\cos w_b}+Y_o\tfrac{\frac{\Phi_b}{\pi}\sin\frac{\Phi_b}{\pi}w_b}{\cos\frac{\Phi_b}{\pi}w_b'-\cos w}\end{aligned}$$

Assuming w on the line M_{a1} in (52) and w on the line M_{b1} in (53), we get two FIEs in $\tilde{V}_{+}(w_a)$ and $\tilde{V}_{\pi+}(w_b)$. We recall that the couple of unknowns $\hat{V}_{+}(w)$, $\hat{V}_{\pi+}(w)$ are different from the couple $\hat{V}_d(w)$, $\hat{V}_{\pi d}(w)$ by a factor $\sin w$.

Efficient approximate methods for the solution of FIEs of second kind are widely available in literature, see for example [40]. Since the kernels of (52) and (53) present well suited behavior, we use a simple sample and hold quadrature scheme to obtain accurate and stable numerical solutions. We apply uniform sampling $f(h\,i)$ with $i=-\frac{A}{h}..\frac{A}{h}$ and modified left-rectangle numerical integration formula $\int_{-\infty}^{\infty}f(u)du\approx h\sum_{i=-A/h}^{A/h}f(h\,i)$ where A and h are respectively the truncation parameter and the step parameter for the integrals in u. This rule has been successfully applied in wedge problems [18],[22],[23]. The total number of samples is $N=2A/h+1$. We observe that as $A\to+\infty$ and $h\to 0$, the numerical

$$\begin{cases} \hat{Y}(w)\,\hat{V}_+(w)+\hat{I}_+(w)+\dfrac{\Phi_a}{2\pi^2 j}\displaystyle\int_{M_{a1}}\dfrac{\left[\tilde{Y}(w_a')-\hat{Y}(w)\right]\tilde{V}_{d+}(w_a')}{\cos(\frac{\Phi_a}{\pi}w_a')-\cos w}dw_a'-\dfrac{\Phi_b}{2\pi^2 j}\displaystyle\int_{M_{b1}}\dfrac{\left[\tilde{Y}(w_b')-\hat{Y}(w)\right]\tilde{V}_{\pi d}(w_b')}{\cos(\frac{\Phi_b}{\pi}w_b')+\cos w}dw_b'=\hat{S}_{tot+}(w) & (48)\\ \hat{Y}(w)\,\hat{V}_{\pi+}(w)-\hat{I}_{\pi+}(w)+\dfrac{\Phi_b}{2\pi^2 j}\displaystyle\int_{M_{b1}}\dfrac{\left[\tilde{Y}(w_b')-\hat{Y}(w)\right]\tilde{V}_{\pi d}(w_b')}{\cos(\frac{\Phi_b}{\pi}w_b')-\cos w}dw_b'-\dfrac{\Phi_a}{2\pi^2 j}\displaystyle\int_{M_{a1}}\dfrac{\left[\tilde{Y}(w_a')-\hat{Y}(w)\right]\tilde{V}_{d}(w_a')}{\cos(\frac{\Phi_a}{\pi}w_a')+\cos w}dw_b'=\hat{S}_{tot\pi+}(w) & (49)\end{cases}$$

$$\begin{cases} \hat{G}(w)\,\hat{V}_+(w)+\dfrac{1}{2\pi j}\displaystyle\int_{M_{a1}}\hat{H}_{11}(w_a,w_a')\tilde{V}_d(w_a')dw_a'+\dfrac{1}{2\pi j}\displaystyle\int_{M_{b1}}\hat{H}_{12}(w_b,w_b')\tilde{V}_{\pi d}(w_b')dw_b'=\hat{S}_{tot+}(w)-\hat{I}_{NC}(w) & (52)\\ \hat{G}(w)\,\hat{V}_{\pi+}(w)+\dfrac{1}{2\pi j}\displaystyle\int_{M_{a1}}\hat{H}_{21}(w_a,w_a')\tilde{V}_d(w_a')dw_a'+\dfrac{1}{2\pi j}\displaystyle\int_{M_{b1}}\hat{H}_{22}(w_b,w_b')\tilde{V}_{\pi d}(w_b')dw_b'=\hat{S}_{tot\pi+}(w) & (53)\end{cases}$$

solution of the FIE converges to the exact solution [40]; consequently h has to be chosen as small as possible and A has to be chosen as large as possible. In the present problem we have two integrals for each integral equations, whose kernels behave in different ways, thus two discretization schemes are needed. We set parameters A_a, h_a for integrals in w_a along line M_{a1} and parameters A_b, h_b for integrals in w_b along M_{b1}. According to our experience the integral in w_x related to small Φ_x needs more samples to converge: for example if $\Phi_a > \Phi_b$, the integrals along the line M_{a1} is less critical then the one along along M_{b1} thus $A_a < A_b$ and $h_a > h_b$.

The numerical approximation of (52) and (53) yields samples of $\tilde{V}_+(w_a)$, $\tilde{V}_{\pi+}(w_b)$ respectively for $Re[w_a]=-\pi/2$ and $Re[w_b]=-\pi/2$. The approximate solution $\tilde{V}_+(w_a)$ ($\tilde{V}_{\pi+}(w_b)$) reconstructed from the samples via (52)-(53) is valid for a strip of regularity that is at most $-3\pi/2 < Re[w_a] < 0$ ($-3\pi/2 < Re[w_b] < 0$), because the discretization of kernel in (52) ((53)) yields spurious poles in $Re[w_a] = -3\pi/2$ ($Re[w_b] = -3\pi/2$). In order to evaluate asymptotically the electromagnetic field (Section IV) we need to extend the analytical solution obtained by this discretization, see Appendix A. For details on the practical values of integration parameters see Section V. While discretizing (52) and (53) in w_a and w_b planes we need to pay particular attention to the definition of the polydrome function ξ and the integration paths. Looking at this property in the η domain we note that the integration paths M_1, M_{a1} and M_{b1} are as reported in Fig. 2 together with the curves $Im[\xi] = 0$, $Re[\xi] = 0$ and the canonical vertical branch lines of ξ. Although the w plane avoids the presence of the branch line/multi-sheets of ξ by expanding the domain with respect to the η plane (*i.e.* the multi-sheets of ξ in η are reported in a unique w plane), in order to correctly evaluate (52) and (53) via numerical discretization the integration paths must not cross branch lines of ξ. This is effected by selecting as branch lines the unconventional $Re[\xi] = 0$ as automatically done in ©Wolfram Mathematica.

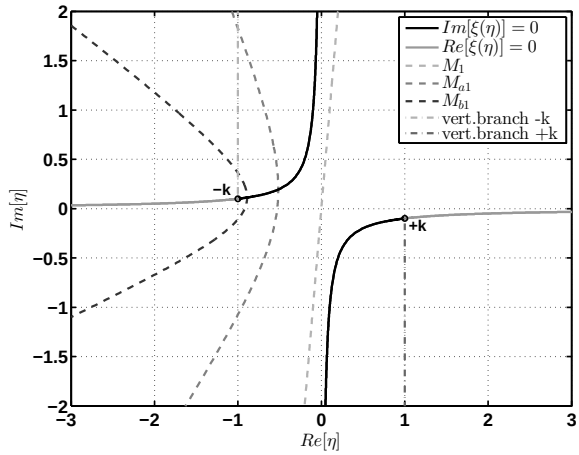

Fig. 2. Possible branch lines of ξ and integration paths M_1, M_{a1} and M_{b1} in the η plane for $\Phi_a = 0.65\pi_{rad}$, $\Phi_b = 0.3\pi_{rad}$, $k = 1 - 0.1j$.

IV. Far Field

A. Angular regions

The estimation of axial spectral unknowns $\hat{V}_d(w), \hat{I}_+(w)$ and $\hat{V}_{\pi d}(w), \hat{I}_{\pi+}(w)$ provide the Laplace transforms in the w plane of the electromagnetic field on the real axis $y = 0$ respectively for $\varphi = 0$ and $\varphi = -\pi$. Given the axial spectra we can obtain the spectra in every direction of the space.

For angular regions, the spectra for any direction φ is obtained through the following expressions [20], [22]. In region 1 we have

$$\begin{cases} \hat{V}_d(w,\varphi) = \frac{Z_o(\hat{I}_+(w-\varphi)-\hat{I}_+(w+\varphi))+\hat{V}_d(w-\varphi)+\hat{V}_d(w+\varphi)}{2} \\ I_+(w,\varphi) = \frac{Z_o(\hat{I}_+(w-\varphi)+\hat{I}_+(w+\varphi))+\hat{V}_d(w-\varphi)-\hat{V}_d(w+\varphi)}{2} \end{cases} \quad (54)$$

for $0 \le \varphi \le \Phi_a$, where $\hat{V}_d(w,\varphi) = \sin w\hat{V}_+(w,\varphi) = \sin wV_+(-k\cos w,\varphi)$ and $\hat{I}_+(w,\varphi) = I_+(-k\cos w,\varphi)$ and, according to (2), (4) and Section III, they are respectively an odd function and an even function of w. Similarly we get

$$\begin{cases} \hat{V}_{\pi d}(w,\bar{\varphi}) = \frac{Z_o(\hat{I}_{\pi+}(w+\bar{\varphi})-\hat{I}_{\pi+}(w-\bar{\varphi}))+\hat{V}_{\pi d}(w+\bar{\varphi})+\hat{V}_{\pi d}(w-\bar{\varphi})}{2} \\ \hat{I}_{\pi+}(w,\bar{\varphi}) = \frac{Z_o(\hat{I}_{\pi+}(w+\bar{\varphi})+\hat{I}_{\pi+}(w-\bar{\varphi}))+\hat{V}_{\pi d}(w+\bar{\varphi})-\hat{V}_{\pi d}(w-\bar{\varphi})}{2} \end{cases} \quad (55)$$

in region 3 for $0 \le \bar{\varphi} \le \Phi_b$ ($\bar{\varphi} = -\pi - \varphi$) and where $\hat{V}_{\pi d}(w,\bar{\varphi}) = \sin w\hat{V}_{\pi+}(w,\bar{\varphi}) = \sin wV_{\pi+}(-k\cos w,\bar{\varphi})$ and $\hat{I}_{\pi+}(w,\bar{\varphi}) = I_{\pi+}(-k\cos w,\bar{\varphi})$ are respectively an odd function and an even function of w.

Starting from region 1, the exact total field is given by the following inverse Laplace-w transforms:

$$\begin{aligned} E_z(\rho,\varphi) &= \tfrac{k}{2\pi}\textstyle\int_{\lambda(B_r)}\hat{V}_+(w,\varphi)e^{jk\rho\cos w}\sin w dw \\ H_\rho(\rho,\varphi) &= \tfrac{k}{2\pi}\textstyle\int_{\lambda(B_r)}\hat{I}_+(w,\varphi)e^{jk\rho\cos w}\sin w dw \end{aligned} \quad (56)$$

where $\lambda(B_r)$ is the mapping of the Bromwich B_r contour of the η-plane into the w-plane, see [20], [22] for details.

By applying the steepest descent path (SDP) method to equations (56), the total field is composed as in (57):

$$E_z(\rho,\varphi) = E_z^g(\rho,\varphi) + E_z^d(\rho,\varphi) + E_z^s(\rho,\varphi) + E_z^l(\rho,\varphi) \quad (57)$$

In (57) the contributions of poles give GO components $E_z^g(\rho,\varphi)$ (58) (non-structural singularities) and possible surface waves $E_z^s(\rho,\varphi)$ (structural singularities), whereas the

branch points are related to lateral waves $E_z^l(\rho,\varphi)$ (structural singularities), and the integral along the SDP (59) is the diffracted component $E_z^d(\rho,\varphi)$.

In this paper we focus our attention on the estimation of GO components and uniform diffracted components (UTD), since in this problem surface waves are not present and for regions with sources in the less dense medium the branch lines give weak contributions $E_z^l(\rho,\varphi)$. Therefore we concentrate our studies and numerical results on (58) and (59):

$$E_z^g(\rho,\varphi) = -jk\sum_i \mathrm{Res}[\hat{\mathrm{V}}_\mathrm{d}(\mathrm{w},\varphi)]_{\mathrm{w_i}(\varphi)}\ \mathrm{e}^{+\mathrm{jk}\rho\cos\mathrm{w_i}(\varphi)} \tag{58}$$

$$E_z^d(\rho,\varphi) = -\frac{ke^{-jk\rho}}{2\pi}\int_{\mathrm{SDP}} \hat{V}_d(w,\varphi)e^{k\rho h(w)}dw \tag{59}$$

where $h(w) = k\rho(\cos w + 1)$, $w_i(\varphi) = w_{oi} \pm \varphi$ and w_{oi} are the poles of the axial spectrum $\hat{V}_d(w)$.

As an alternative, classical GO considerations can be used to obtain the GO components. For regions 1 and 3 we need to consider that the polar reference system is centered in $(x,y) = (0,0)$, thus for each ray (incident, reflected, double reflected...) we need to take into account the different propagation paths with delay and attenuation corrections with respect to the incident field (1) (see test case 2.1).

The SDP integral in (59) represents the diffracted field E_z^d. Since on the SDP $h(w)$ is a continuous real function, which rapidly goes to $-\infty$ toward the end points of the path, as $k\rho \to \infty$, the main contribution in (59) is located near the saddle point $-\pi$, thus the diffracted component can be approximated with the GTD component. For region 1

$$E_z^{gtd}(\rho,\varphi) = E_o\frac{e^{-j(k\rho+\frac{\pi}{4})}}{\sqrt{2\pi k\rho}}D_1(\varphi,\varphi_o) \tag{60}$$

$$D_1(\varphi,\varphi_o) = \frac{-k\hat{V}_d(-\pi,\varphi)}{jE_o} \tag{61}$$

where $\hat{V}_d(-\pi,\varphi)$ is defined in (54). This expression makes the importance of the recursive equations in Appendix A clear. In fact, to estimate $\hat{V}_d(-\pi,\varphi)$ in $0<\varphi<\Phi_a$, we need the axial spectra defined in the range $-\pi-\Phi_a < w < -\pi+\Phi_a$.

Uniform expressions of the total far field $E_z^{tot} = E_z^g + E_z^{utd}$ are obtained through the Uniform Theory of Diffraction (UTD), which removes the caustics of GTD [41]:

$$E_z^{utd}(\rho,\varphi) = E_o\frac{e^{-j\left(k\rho+\frac{\pi}{4}\right)}}{\sqrt{2\pi k\rho}}C_1(\varphi,\varphi_o) \tag{62}$$

$$C_1(\varphi,\varphi_o) = D_1(\varphi,\varphi_o) + \sum_q \Gamma_q \frac{1-F\left(2k\rho\cos^2\frac{\varphi-\varphi_q-\pi}{2}\right)}{\cos\frac{\varphi-\varphi_q-\pi}{2}} \tag{63}$$

where Γ_q are the coefficients of the GO components of direction φ_q and the function $F(z)$ is the Kouyoumjian-Pathak transition function defined in [41] and its application in the framework of WH formulations is reported in (63) of [18].

Concerning region 3, as already discussed in Section III.B, the axial spectra $(\hat{V}_{\pi+}(w), \hat{I}_{\pi+}(w))$ do not contain any non-structural GO poles. This yields the result that the main contribution of the inverse Laplace-w transform of the π spectra is the diffracted field that arises from the integration along the SDP:

$$E_z^d(\rho,\varphi) = -\frac{ke^{-jk\rho}}{2\pi}\int_{\mathrm{SDP}} \hat{V}_{\pi d}(w,-\pi-\varphi)e^{k\rho h(w)}dw \tag{64}$$

for $-\pi-\Phi_b < \varphi < -\pi$. Since there are no poles in the spectra, no shadow regions are present, thus uniform theory (UTD) is not necessary for this region and E_z^d represents the total field. As $k\rho \to \infty$, the main contribution in (64) is located near the saddle point $-\pi$, yielding the GTD component:

$$E_z^{gtd}(\rho,\varphi) = E_o\frac{e^{-j(k\rho+\frac{\pi}{4})}}{\sqrt{2\pi k\rho}}D_3(\varphi,\varphi_o) \tag{65}$$

$$D_3(\varphi,\varphi_o) = \frac{-k\hat{V}_{\pi d}(-\pi,-\pi-\varphi)}{jE_o} \tag{66}$$

with $\hat{V}_{\pi d}(-\pi,\varphi)$ defined in (55).

B. Layered region

With reference to Fig. 1, the Fourier transform along x of the total electric field E_z for $y<0$ is reported in (14) and (15). From these expressions it is possible to evaluate the total field in any point of region 2 by using the inverse Fourier transform

$$E_z(x,y) = \frac{1}{2\pi}\int_{-\infty}^{\infty} v(\eta,y)e^{-j\eta x}d\eta \tag{67}$$

that can be re-written in terms of inverse Laplace transforms

$$\begin{array}{l} E_z(x,y) = \frac{1}{2\pi}\int_{B_+} v_+(\eta,y)e^{-j\eta x}d\eta,\ (x>0, y<0) \\ E_z(x,y) = \frac{1}{2\pi}\int_{B_-} v_-(\eta,y)e^{-j\eta x}d\eta,\ (x<0, y<0) \end{array} \tag{68}$$

where B_+ (B_-) is a horizontal line located above (under) the singularities of $v_+(\eta,y)$ ($v_-(\eta,y)$) and where $v(\eta,y)$ is decomposed into $v(\eta,y) = v_-(\eta,y) + v_+(\eta,y)$ [26] .

The estimation of far field is obtained for $y<-d$ through the inverse transform of (15), where

$$v(\eta,-d) = \frac{Y_c(\eta)\left[V_+(\eta)+V_{\pi+}(-\eta)\right]}{Y_c(\eta)\cos(\xi d) + jY_d(\eta)\sin(\xi d)} \tag{69}$$

with $\xi = \xi(\eta)$, $v_+(\eta,0) = V_+(\eta)$ and $v_-(\eta,0) = V_{\pi+}(-\eta)$. Using asymptotic estimation of (68) with the SDP method, the total far field in the homogeneous dielectric half-space is constituted by the GO component and the diffracted component:

$$E_z^d(\rho',\varphi') = E_o\sqrt{\frac{1}{2\pi k_d\rho}}e^{-j(k_d\rho+\pi/4)}D_2(\varphi',\varphi_o) \tag{70}$$

The GO component can be obtained via the residue theorem or via classical GO considerations. For region 2 we need to consider that the polar reference system is centered in $(x,y) = (0,-d)$, thus for each ray (directly transmitted, reflected and transmitted ...) we need to take into account the different propagation paths with phase and attenuation corrections with respect to the incident field(see test case 2.1).

In (70) the polar reference system (ρ',φ') is centered in the cartesian coordinate $(0,-d)$ with $-\pi<\varphi'<0$ (see Fig. 1). The GTD diffraction coefficient is given by

$$D_2(\varphi',\varphi_o) = \frac{k_d v(k_d\cos\varphi',-d)\sin\varphi'}{jE_o} \tag{71}$$

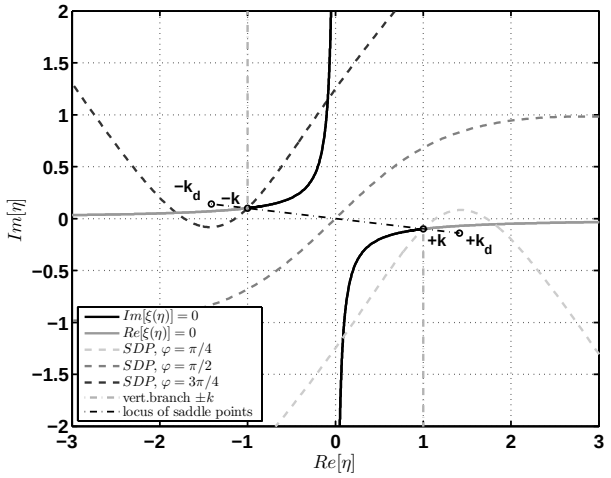

Fig. 3. Locus of saddle points $k_d \cos\varphi'$, possible branch lines of ξ and SDP curves as a function of φ' for $k = 1 - 0.1j$ and $\varepsilon_r = 2$.

where $\eta_s = k_d \cos\varphi'$ is the saddle point. We note that the GTD diffraction coefficient depends on the spectra of $V_+(\eta)$, $V_{\pi+}(-\eta)$ that are computed through $\hat{V}_+(w)$, $\hat{V}_{\pi+}(w)$ using the inverse mapping between w and η planes (Appendix I of [18]):

$$w(\eta) = \begin{cases} -j\log\left(\frac{\eta+j\xi}{k}\right) - \pi, & Arg\left[\frac{\eta+j\xi}{k}\right] > -\frac{\pi}{2} \\ -j\log\left(\frac{\eta+j\xi}{k}\right) + \pi, & Arg\left[\frac{\eta+j\xi}{k}\right] \leq -\frac{\pi}{2} \end{cases} \quad (72)$$

In (71) we need to compute $V_+(k_d\cos\varphi')$ and $V_{\pi+}(-k_d\cos\varphi')$ for $-\pi < \varphi' < 0$. For $\varphi' > -\arccos(1/\sqrt{\varepsilon_r})$ and $\varphi' < -\arccos(-1/\sqrt{\varepsilon_r})$ we obtain corresponding non-real values of w (for a deeper discussion see test case 2.1 of Section V and in particular Fig. 12). Another important implementation aspect in (71) is that, in order to correctly evaluate $v(\eta, -d)$ in the saddle point η_s, the approximated axial spectra must be reconstructed numerically via (52) and (53) by selecting a suitable determination of polydrome function ξ. In this case, during the reconstruction of the spectral unknowns, we need to select as branch lines the vertical lines starting from $\pm k$ to avoid crossing of branch lines by SDP paths, see Fig. 3 for these curves. Note that this selection is different from the one made in the numerical integration of (52) and (53) in Section III (see at the end of the section). This choice avoids cumbersome computation with saddle points η_s in the improper sheet of ξ in the η plane. The mapping (72) together with the choice of vertical branch lines for ξ is of fundamental importance to correctly compute $D_2(\varphi', \varphi_o)$ by linking it to the axial spectra $\hat{V}_+(w)$, $\hat{V}_{\pi+}(w)$.

V. Validation and Numerical results

The efficiency, the convergence and the validation of the proposed approximate solution is illustrated through several test problems. The quantities used in this section are explicitly defined in the previous sections.

All the test cases make reference to Fig. 1 for the geometry. In particular, the wedge is illuminated by a plane wave (1) impinging from a direction φ_o with $0 < \varphi_o < \Phi_a$ (leaving the wedge with direction $\varphi_I = -\pi + \varphi_o$).

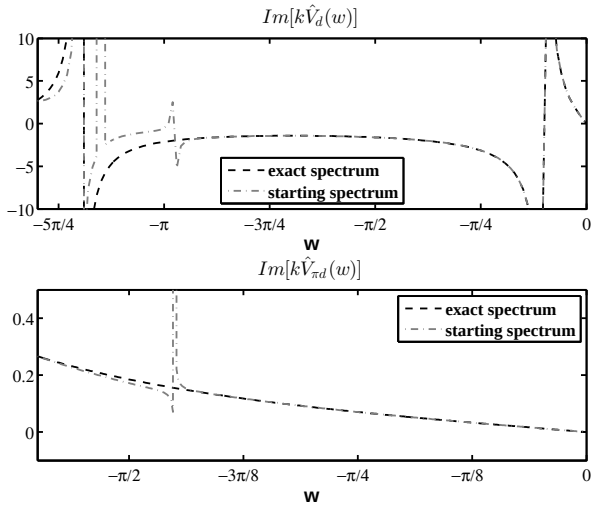

Fig. 4. Test case 1.1: imaginary parts of the exact spectra compared with the approximated starting spectra: on top $k\hat{V}_d(w)$ in $-2\Phi_a \leq w \leq 0$, on bottom $k\hat{V}_{\pi d}(w)$ in $-2\Phi_b \leq w \leq 0$. Note the loss of convergence respectively at $w = -3\Phi_a/2$ and $w = -3\Phi_b/2$.

A comparison with the exact solution is only possible in the free space limit ($\varepsilon_r = 1$). This problem is the first test case, where a deep study on the convergence is taken into account in terms of spectra, GTD coefficient, total far field as a function of integration parameters (A_a, h_a, A_b, h_b) in the numerical implementation of (52) and (53).

The following test cases (see Table I) examine in details the arbitrarily oriented PEC wedge over a dielectric half-space for different

- directions of incident plane wave,
- aperture angles Φ_a and Φ_b (acute and obtuse),
- values of the distance d (with limit case $d = 0$)
- values of rel. permittivity ε_r (with limit case $\varepsilon_r = 1$).

Solutions are reported in terms of spectra, GTD coefficient, UTD field, total far field.

Self-convergence is studied in detail in test case 2, the overall test cases show the effectiveness of the proposed method for arbitrary values of ε_r, d, Φ_a, Φ_b, φ_o.

In this paper we denote the azimuthal direction of the GO waves with φ_{lab} where the subscripts lab are in upper case (lower case) if referring to a wave that leaves (approaches) the wedge: for instance, the face a reflected wave propagates as $e^{jk\rho\cos(\varphi-\varphi_{ra})} = e^{-jk\rho\cos(\varphi-\varphi_{RA})}$ with $\varphi_{ra} = 2\Phi_a - \varphi_o$ and $\varphi_{RA} = \varphi_{ra} - \pi$. In the examples we assume small loss, thus the free-space propagation constant is $k = k_r - jk_i$ with $k_i = 0.01k_r$. In the following, we consider all the angles in $radiants$ by omitting rad and $|E^i| = 1V/m$.

TABLE I
Test cases

n.	ε_r	d	Φ_a	Φ_b	φ_o
1.1	1	any	$0.65\pi_{rad}$	$0.3\pi_{rad}$	$0.1\pi_{rad}$
1.2	1	any	$0.65\pi_{rad}$	$0.3\pi_{rad}$	$0.55\pi_{rad}$
1.3	1	any	$0.65\pi_{rad}$	$0.3\pi_{rad}$	$0.4\pi_{rad}$
2.1	4	$\lambda/4$	$0.65\pi_{rad}$	$0.3\pi_{rad}$	$0.55\pi_{rad}$
2.X	4	$[0, 4\lambda/5]$	$0.65\pi_{rad}$	$0.3\pi_{rad}$	$0.55\pi_{rad}$
3	$[1, 10]$	$\lambda/5$	$0.45\pi_{rad}$	$0.4\pi_{rad}$	$0.25\pi_{rad}$

$$\begin{cases} \hat{V}_+^{\text{free}}(w,\varphi) = \dfrac{j\pi \csc(w) \sin\left(\frac{\pi(\Phi_a-\varphi_o)}{\Phi_a+\Phi_b+\pi}\right)\left(\cos\left(\frac{\pi(-\Phi_a+\varphi+w)}{\Phi_a+\Phi_b+\pi}\right)-\cos\left(\frac{\pi(\Phi_a-\varphi+w)}{\Phi_a+\Phi_b+\pi}\right)\right)}{k(\Phi_a+\Phi_b+\pi)\left(\cos\left(\frac{\pi(\Phi_a-\varphi_o)}{\Phi_a+\Phi_b+\pi}\right)-\cos\left(\frac{\pi(\Phi_a-\varphi+w)}{\Phi_a+\Phi_b+\pi}\right)\right)\left(\cos\left(\frac{\pi(-\Phi_a+\varphi+w)}{\Phi_a+\Phi_b+\pi}\right)-\cos\left(\frac{\pi(\Phi_a-\varphi_o)}{\Phi_a+\Phi_b+\pi}\right)\right)} \quad (73) \\ \hat{I}_+^{\text{free}}(w,\varphi) = -\dfrac{j\pi \sin\left(\frac{\pi(\Phi_a-\varphi_o)}{\Phi_a+\Phi_b+\pi}\right)}{kZ_o(\Phi_a+\Phi_b+\pi)}\left(\dfrac{1}{\cos\left(\frac{\pi(-\varphi+w+\Phi_a)}{\Phi_a+\Phi_b+\pi}\right)-\cos\left(\frac{\pi(\Phi_a-\varphi_o)}{\Phi_a+\Phi_b+\pi}\right)}+\dfrac{1}{\cos\left(\frac{\pi(\varphi+w-\Phi_a)}{\Phi_a+\Phi_b+\pi}\right)-\cos\left(\frac{\pi(\Phi_a-\varphi_o)}{\Phi_a+\Phi_b+\pi}\right)}\right) \quad (74) \end{cases}$$

A. Test case 1

The first test case analyzes the arbitrarily oriented PEC wedge in free space, where the closed-form exact solution is available (73)-(74). All the properties of our solution are given in terms of spectral quantities, diffraction coefficients, total far fields. With reference to Fig. 1 the physical parameters of the problem in test case 1.1 are: $\Phi_a = 0.65\pi$, $\Phi_b = 0.3\pi$, $\varepsilon_r = 1$, $\varphi_o = 0.1\pi$, $|E^i| = 1V/m$ and $k = k_r - jk_i$ with $k_i = 0.01k_r$. According to GO, the E-polarized incident plane wave impinges on the wedge and generates shadow boundaries due to the incident wave ($\varphi_I = -\pi + \varphi_o = -0.9\pi$) and the reflected wave from face a ($\varphi_{RA} = -\pi + 2\Phi_a - \varphi_o = 0.2\pi$). We note that the directions of the waves identify also the shadow boundaries. The total far field is reported on top of Fig.7.

The full convergence of the solution of the problem is practically obtained applying the discretization method reported in Section III.C to (52) and (53) where the quadrature parameters are chosen to be $A_a = 40$, $h_a = 0.5$, $A_b = 80$, $h_b = 0.5$ (see below for a discussion on this selection).

With the physical parameters reported above, we note that the source in the system of FIEs (52) and (53) is only composed of some of the terms in (50), (51), (31) depending on the step functions. In this case, and in general for $0 < \varphi_o < \Phi_a/2$, all the terms are present except the one related to $u_a(\varphi_o)$.

Fig.4 shows the behavior of the numerical solution in terms of the imaginary part of the spectral unknowns $k\hat{V}_d(w)$ in $-2\Phi_a \le w \le 0$ and $k\hat{V}_{\pi d}(w)$ in $-2\Phi_b \le w \le 0$ as they are obtained by direct numerical implementation of the system of FIEs (52) and (53). These approximations are called starting spectra and in the figure they are compared with the exact axial spectra. The exact spectra for any φ is reported in (73)-(74) for the free-space case and it is purely imaginary if $k \in \mathbb{R}$.

The approximate starting axial spectra of Fig.4 show spurious poles at $Re[w] = -3\Phi_a/2$ and $Re[w] = -3\Phi_b/2$ respectively for $\hat{V}_d(w)$ and $\hat{V}_{\pi d}(w)$ (see Section III.C). In order to analytically extend the solution we resort to recursive equations as described in Appendix A. For the use of the recursive formulas (80)-(83) we have selected (86) $\gamma = 1.25$ since $\frac{\pi}{\Phi_a+\Phi_b} \simeq 1.053$ and $\frac{\pi}{\Phi_a-\Phi_b} \simeq 2.857$. The trade off on γ is that the lower bound is fine for precision since the spectra is far way from the spurious poles, however this choice is less efficient in terms of recursions.

Fig. 5 shows the behavior of the extended numerical solution in terms of the absolute value of the spectral unknowns $\hat{V}_d(w)$ and $\hat{V}_{\pi d}(w)$ in $-2\pi \le w \le 0$. Relative errors are reported in $\log_{10}$ scale by considering as reference solution the closed-form exact solution. For the numerical solution we have chosen different values of the integration parameter $[A_a, h_a, A_b, h_b]$ in order to confirm the convergence of our technique. However, an excessive value of A_a (A_b) and/or small value of h_a (h_b) yields ill-conditioned matrices in the discretization process. The selection of quadrature parameters $[A_a, h_a, A_b, h_b]$ comes from the study of the bands of the

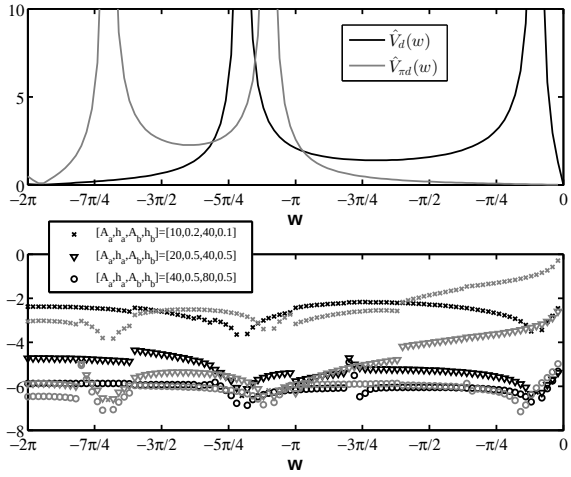

Fig. 5. Test case 1.1: on top absolute values of the approximated spectra $\hat{V}_d(w)$ in black, $\hat{V}_{\pi d}(w)$ in grey for $-2\pi \le w \le 0$ and, on bottom relative errors in log10 scale. The relative errors are computed with respect to the exact solution.

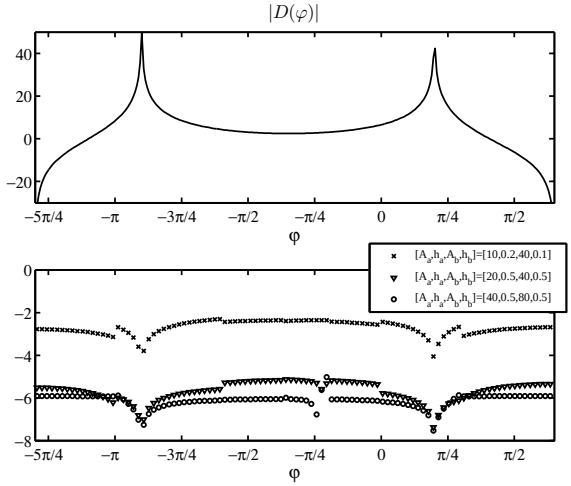

Fig. 6. Test case 1.1: on top the absolute value of GTD diffraction coefficient is reported in dB, on bottom the relative error on the computation of GTD diffraction coefficient in log_{10} scale for different integration parameters with respect to the exact solution.

kernels in w plane and in particular from the validation of the integral equations (48)-(49), (30), (33) and (52)-(53) by replacing inside the integrals the spectra with the known closed-form exact spectra (73)-(74) for the free-space case.

In Fig. 5 $\hat{V}_d(w)$ shows peaks for the incident wave and for the face a reflected wave: $w_I = -\varphi_o = -0.1\pi$ and $w_{RA} = -\varphi_{ra} = -2\Phi_a + \varphi_o = -1.2\pi$. The location of the poles agrees with the standard GO theory: the axial spectra show singularities for $\pm w_X$ (where $w_X = -\pi - \varphi_X$ with $X = I, RA...$) due to symmetry of plus functions in w plane.

According to the GTD diffraction coefficient (61), (66) and (71), we obtain that $\varphi_I = -w_I - \pi = -0.9\pi$ and $\varphi_{RA} = -w_{RA} - \pi = 0.2\pi$. We note that in this particular case of free space we could use (61) as GTD diffraction coefficient in the

homogenous angular region defined by $-\pi - \Phi_b < \varphi_o < \Phi_a$.

The GO components can be obtained by using standard techniques or by applying (58) for homogenous angular regions. Notice that the study of the axial spectra is fundamental. In fact, for example in region 1, if w_{oi} is a singularity of $\hat{V}_+(w)$ ($\hat{I}_+(w)$), the spectrum of $\hat{V}_+(w,\varphi)$ ($\hat{I}_+(w,\varphi)$) presents the singularities $w_i(\varphi) = w_{oi} \pm \varphi$ that can be captured by the integration contour deformation from B_r to SDP, see Sec. IV.

The approximate total GTD diffraction coefficients are estimated substituting the approximations of the spectral unknowns in (61), (66) and (71). On the top of Fig. 6 the absolute value of the total GTD diffraction coefficient is reported in dB for each observation angle φ. The peaks of the GTD diffraction coefficients occur for the GO angles: face a reflected wave $\varphi_{RA} = 0.2\pi$ and incident wave $\varphi_I = -0.9\pi$. On the bottom of Fig. 6 the convergence is shown for different integration parameters through the evaluation of the relative error in $\log_{10}$ scale with respect to the exact solution. This scale measures the precision in term of digits for each observation angle φ.

The complete solution is reported in terms of the total far field, GO field component, UTD field component at the distance $k_r\rho = 10$ on top of Fig. 7. The relative error of $|\mathbf{E_{tot}}|$ in log_{10} scale for $[A_a, h_a, A_b, h_b]$=$[40, 0.5, 80, 0.5]$ with respect to the exact solution is reported on the bottom of Fig.7.

The change of the incident wave angle φ_o conditions the source terms in the system of FIEs (52) and (53), see Section III.C. If $\pi/2 < \varphi_o < \Phi_a$, all the terms in (50), (51), (31) are null except the one that does not depend on the step functions. The complete solution of test case 1.2 is reported on top of Fig. 8 in black in terms of the total field, GO field component, UTD field component for $\varphi_o = 0.55\pi$ at the distance $k_r\rho = 10$ for $[A_a, h_a, A_b, h_b] = [40, 0.5, 80, 0.5]$ and $\gamma = 1.25$.

The last case 1.3 is when $\Phi_a/2 < \varphi_o < \pi/2$: all the terms in (50), (51), (31) are present except the ones depending on $u(\Phi_a/2 - \varphi_o)$. The complete solution of test case 1.3 is reported on top of Fig.8 in grey in terms of the total field, GO field component, UTD field component for $\varphi_o = 0.4\pi$ at the distance $k_r\rho = 10$. On the bottom of Fig.8 the relative error of $|\mathbf{E_{tot}}|$ in log_{10} scale is reported with respect to the exact solution for test cases 1.2 and 1.3.

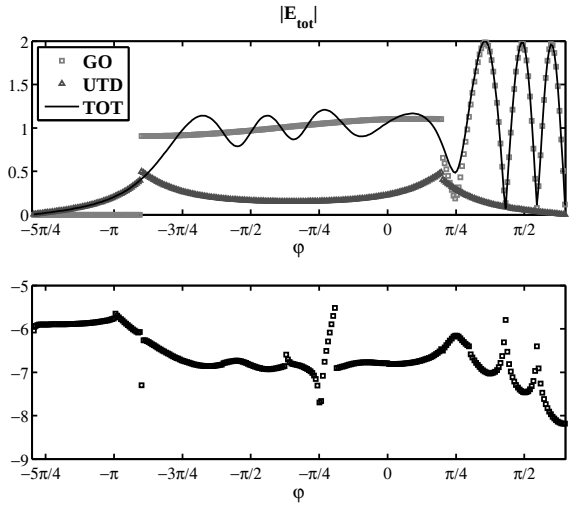

Fig. 7. Test case 1.1 with $\varphi_o = 0.1\pi$: on top the GO field, the UTD component and, the total far-field pattern at $k_r\rho = 10$, on the bottom the relative error of $|\mathbf{E_{tot}}|$ in log_{10} scale for $[A_a, h_a, A_b, h_b] = [40, 0.5, 80, 0.5]$ with respect to the exact solution.

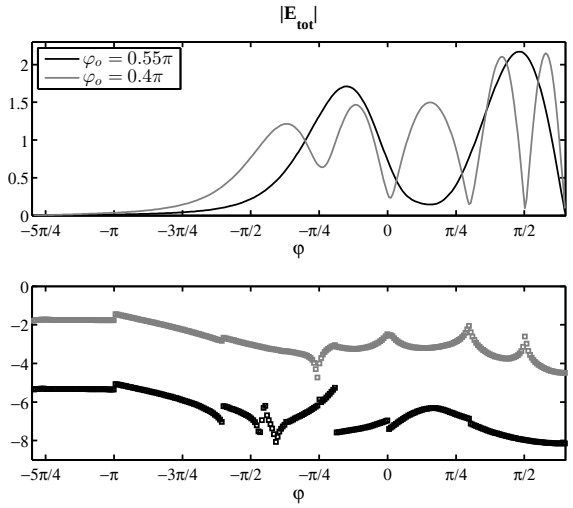

Fig. 8. Test case 1.2 with $\varphi_o = 0.55\pi$ in black, test case 1.3 with $\varphi_o = 0.4\pi$ in grey: on top the GO field, the UTD component and, the total far-field pattern at $k_r\rho = 10$, on bottom the relative error of $|\mathbf{E_{tot}}|$ in log_{10} scale for $[A_a, h_a, A_b, h_b] = [40, 0.5, 80, 0.5]$ with respect to the exact solution.

B. Test case 2

With reference to Fig. 1 the physical parameters of the problem test case 2.1 are: $\varepsilon_r = 4$, $d = \lambda/4$, $\Phi_a = 0.65\pi$, $\Phi_b = 0.3\pi$, $\varphi_o = 0.55\pi$, $|E^i| = 1V/m$ and $k = k_r - jk_i$ with $k_i = 0.01k_r$.

For this problem no exact solution is available, thus we have studied self-convergence. The solution is given in terms of approximate spectra, diffraction coefficients and total fields.

According to GO, the E-polarized incident plane wave impinges on the wedge and thus on the dielectric half-space, by generating two reflected waves and two transmitted waves.

In region 1 the GO field is composed of the incident wave, the face a reflected wave with direction $\varphi_{RA} = -\pi + \varphi_{ra} = -\pi + 2\Phi_a - \varphi_o = -\pi/4$, the directly reflected wave from the dielectric half-space with direction $\varphi_{RD} = \pi - \varphi_o = 0.45\pi$ and the double reflected wave (first from the face a and then from the dielectric half-space) with direction $\varphi_{RDRA} = \pi - \varphi_{ra} = 0.25\pi$ (where $\varphi_{ra} = 2\Phi_a - \varphi_o$). In region 2 the GO field is composed of the directly transmitted wave through the dielectric half-space with direction $\varphi_{TD} = -\arccos(-\frac{1}{\sqrt{\varepsilon_r}}\cos(\varphi_o)) \simeq -0.475\pi$ and the transmitted wave from the reflected wave of face a with direction $\varphi_{TDRA} = -\arccos(-\frac{1}{\sqrt{\varepsilon_r}}\cos(\varphi_{ra})) \simeq 0.385\pi$.

We note that the direction of the waves also identifies the shadow boundaries. Moreover, while making classical GO considerations, we need to take into account the different paths of the rays and the local reference system. For regions 1 and 3 the polar reference system is centered in $(x, y) = (0, 0)$, while for region 2 it is centered in $(x, y) = (0, -d)$. To correctly compute the GO field, each ray (incident (I), reflected from face a (RA), reflected from dielectric (RD), double reflected from face a and dielectric (RDRA), transmitted through the dielectric (TD), reflected from face a and transmitted through dielectric (TDRA)) must be computed with phase and attenuation corrections with respect to the phase center of the incident

field (1) which is $(x, y) = (0, 0)$, see (75).

The convergence of the solution of the problem is obtained by applying the discretization method reported in Section III.C to (52) and (53), where the quadrature parameters are chosen to be $[A_a, h_a, A_b, h_b] = [10, 0.2, 40, 0.1]$. This selection comes from the study of the bands of the kernels in w plane and in particular from our experience in the convergence of the free-space case (test case 1).

$$\begin{cases} E_z^{\text{RA}} = \Gamma_{\text{RA}} e^{jk\rho\cos(\varphi-\varphi_{ra})} \\ E_z^{\text{RD}} = \Gamma_{\text{RD}} e^{jk\rho\cos(\varphi-\varphi_{rd})} e^{jk2d\sin(\varphi_o)} \\ E_z^{\text{RDRA}} = \Gamma_{\text{RDRA}} e^{jk\rho\cos(\varphi-\varphi_{rdra})} e^{jk2d\sin(\varphi_{ra})} \\ E_z^{\text{TD}} = T_{\text{TD}} e^{jk\rho\cos(\varphi-\varphi_{td})} e^{jk(-d\sin(\varphi_o))} \\ E_z^{\text{TDRA}} = T_{\text{TDRA}} e^{jk\rho\cos(\varphi-\varphi_{tdra})} e^{jk(-d\sin(\varphi_{ra}))} \end{cases} \tag{75}$$

With the physical parameters reported above, we note that the source in the system of FIEs (52) and (53) is only composed of some of the terms in (50), (51), (31) depending on the step functions. In this case, and in general for $\pi/2 < \varphi_o < \Phi_a$, all the terms in (50), (51), (31) are null except the one that does not depend on the step functions.
Since Φ_a and Φ_b are not changed from test case 1 we choose the same value of $\gamma = 1.25$ for the recursive formulas (80)-(83).

Fig. 9 shows the behavior of the numerical solution in terms of the absolute value of the axial spectral unknowns $\hat{V}_d(w)$, $\hat{V}_{\pi d}(w)$ in $-2\pi \leq w \leq 0$ compared with the ones obtained without dielectric half-space (free space). In particular $\hat{V}_d(w)$ show peaks for the directly reflected wave from the dielectric half-space $w_{RD} = -\varphi_o = -0.55\pi$ and for double reflected wave (first from the face a and then from the dielectric half-space) $w_{RDRA} = -2\Phi_a + \varphi_o = -0.75\pi$. The location of the poles agrees with the standard GO theory: the axial spectra show singularities for $\pm w_X$ (where $w_X = -\pi - \varphi_X$ with $X = I, RA, RD, RARD...$) due to symmetry of plus functions in w plane. As expected no peaks occurs in the spectrum of $\hat{V}_{\pi d}(w)$ in $-2\pi \leq w \leq 0$ (Sec. IV.A and III.B).

The GTD diffraction coefficient is derived from (61), (66) and (71), and reported in dB on top of Fig. 10 for each observation angle φ. The layered region 2 is highlighted in grey to make clear the reference system in use for the GTD coefficient which is centered in $O' = (x, y) = (0, -d)$ in region 2 and in $O = (x, y) = (0, 0)$ in regions 1 and 3 (see Fig. 1). As expected peaks are shown for $\varphi = \varphi_{RD}, \varphi_{RDRA}$ in region 1 and for $\varphi = \varphi_{TD}, \varphi_{TDRA}$ in region 2, no GO peaks in region 3. On the bottom of Fig. 10 the study of self-convergence is reported based on the computation of relative errors. Relative errors are reported in linear scale by considering as reference solution the one obtained for $[A_a, h_a, A_b, h_b] = [10, 0.2, 40, 0.1]$. We have selected different values of the integration parameter $[A_a, h_a, A_b, h_b]$ in order to confirm the convergence of our technique. However, an excessive value of A_a (A_b) and/or small value of h_a (h_b) yields ill-conditioned matrices in the discretization process.

Fig. 11 reports the numerical estimations of the GO field, the UTD component and the total far field at the distance $k_r\rho = 10$ from the edge of the wedge. The layered region 2 is highlighted in grey to make clear the reference system in

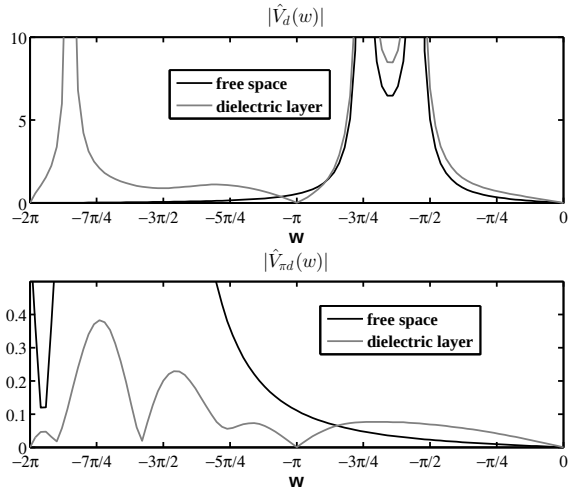

Fig. 9. Test case 2.1: the absolute value of the approximated spectra $\hat{V}_d(w)$ and $\hat{V}_{\pi d}(w)$ are reported for $-2\pi \leq w \leq 0$ respectively on top and on bottom of the figure.

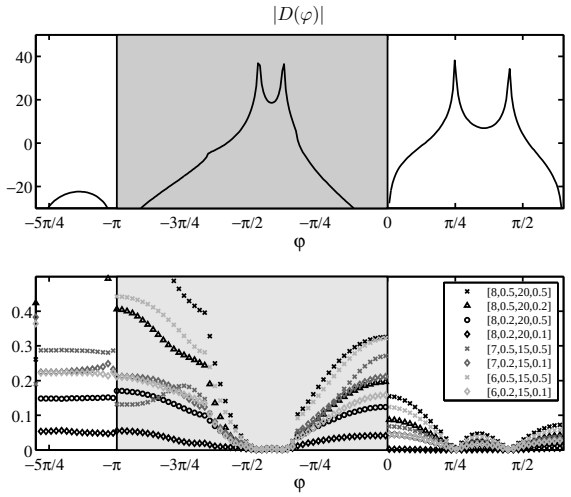

Fig. 10. Test case 2.1: on top the absolute value of the GTD diffraction coefficient, on bottom the relative error on the computation of the GTD diffraction coefficient in linear scale for different integration parameters $[A_a, h_a, A_b, h_b]$ with respect to the reference solution obtained for $[A_a, h_a, A_b, h_b] = [10, 0.2, 40, 0.1]$.

use for the total far field, which is centered in $O' = (x, y) = (0, -d)$ in region 2 and in $O = (x, y) = (0, 0)$ in regions 1 and 3 (see Fig. 1). Fig. 11 also highlights the UTD component with a probable loss of precision in two points (black arrows)

$$\varphi_{+k,-k} = -\arccos(\pm 1/\sqrt{\varepsilon_r}) = -\pi/3, -2\pi/3 \tag{76}$$

due to the evaluation of the GTD coefficient in region 2 (71). The computation of (71) requires the estimation of $v(k_d \cos\varphi', -d)$ which is directly related to the axial spectra $\hat{V}_+(w)$ and $\hat{V}_{\pi+}(w)$ through (69). For $\varphi > \varphi_{+k}$ and $\varphi < \varphi_{-k}$ $\hat{V}_+(w)$ and $\hat{V}_{\pi+}(w)$ are computed in complex values of the plane w and in particular the mapping

$$k_d \cos(\varphi) = \pm\eta = \mp k \cos w \tag{77}$$

based on (72) show kinks at $\varphi_{\pm k}$. Fig. 12 illustrates the mapping between φ and w that relates the GTD coefficient in region 2 (71) and $\hat{V}_+(w)$. The same figure can be read in

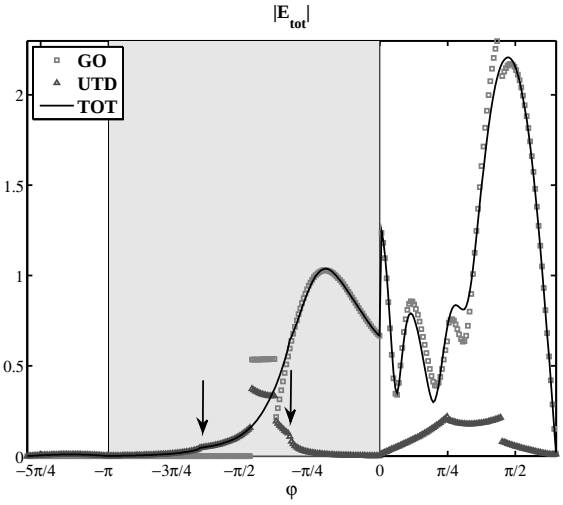

Fig. 11. Test case 2.1: the GO field, the UTD component and, the total far-field pattern at $k_r\rho = 10$.

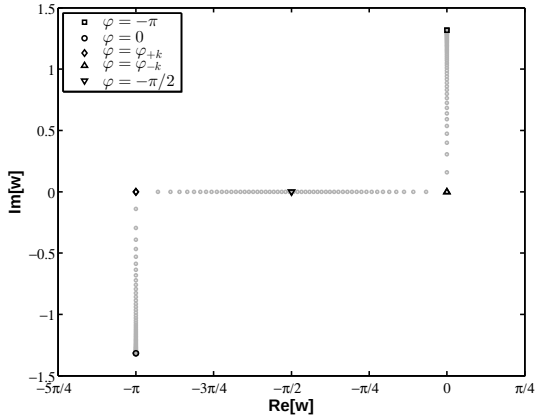

Fig. 12. Test case 2.1: mapping between φ of the GTD coefficient in region 2 (71) and w of $\hat{V}_+(w)$.

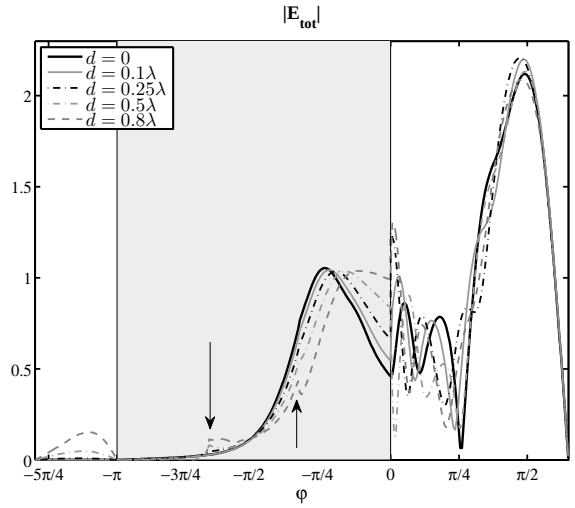

Fig. 13. Test case 2.X: the total far-field pattern at $k_r\rho = 10$ for different values of d. The figure shows a loss in precision for $\varphi_{+k,-k}$ (76) especially for increasing values of d, highlighted thorough arrows.

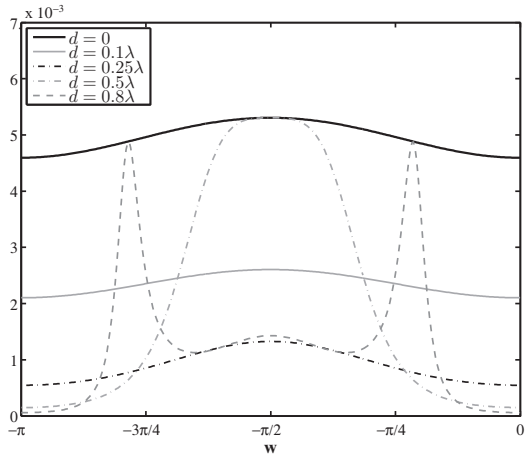

Fig. 14. Test case 2.X: real part of $\hat{Y}_d(w)$ as a function of the distance d. Similar dynamics is obtained for the imaginary part.

opposite sense to illustrate the mapping between φ and w that relates (71) and $\hat{V}_{\pi+}(w)$ interchanging π with 0 and φ_{+k} with φ_{-k}. As shown in Fig. 12 uniform sampling in φ corresponds to non-uniform sampling in w and this property conditions the numerical properties of the solution especially near the kinks.

Fig. 13 reports the numerical estimations for test case 2.X of the total far field at the distance $k_r\rho = 10$ from the edge of the wedge for different values of d from $d = 0$ to $d = 0.8\lambda$ which is almost far distance since $k_r d > 5$. As already noted in Fig. 11, Fig. 13 shows a loss in precision for $\varphi_{+k,-k}$ (76) especially for increasing values of d. However the scope of our paper is to model the near-field interaction of a wedge and a dielectric half-space. For values of $d > 0.8\lambda$ the wedge and the dielectric half-space interact in far zone thus our formulation that involves a unique entire model of the problem is not needed in this case. However we think that the loss of precision for $d > 0.8\lambda$ is due to the high dynamics of the admittance $\hat{Y}_d(w) = Y(-k\cos(w)$ (10) in the w plane (see Fig. 14 for the real part of $\hat{Y}_d(w)$) that requires a local estimation of the samples of the axial spectra for values of w different from what is obtained in the numerical solution of FIEs (52) and (53) where the samples of $\hat{V}_d(w)$ and $\hat{V}_{\pi d}(w)$ are respectively localized at M_{a1} and M_{b1}. As discussed in Section III FIE formulations can be obtained for any integration vertical line of the w plane, taking care of structural and non structural singularities. However for near-field interaction $(d < 0.8\lambda)$ we recall that the use of recursive equations (80)-(83) yields high precision results in terms of approximate spectra in the entire w plane.

C. Test case 3

With reference to Fig. 1 the physical parameters of test case 3 are: $d = \lambda/5$, $\Phi_a = 0.45\pi$, $\Phi_b = 0.4\pi$, $\varphi_o = 0.25\pi$, $|E^i| = 1V/m$ and $k = k_r - jk_i$ with $k_i = 0.01k_r$. Note that both angular regions 1 and 3 are acute.

The solution is given in terms of approximate diffraction coefficients and total fields for different values of dielectric constants ε_r: from low contrast ($\varepsilon_r = 1.001$) to high contrast ($\varepsilon_r = 10$).

According to GO, the E_z-polarized incident plane wave impinges on the wedge twice: directly and after reflection from the dielectric half-space thus generating two double reflected waves in region 1 and two transmitted waves in region 2. In

the following the formulas are for a general value of relative dielectric constant ε_r, while the values refers to $\varepsilon_r = 2$.

In region 1 the GO field is composed of the incident field, the reflected waves from face a and the dielectric half-space together with the double reflected wave (first from the face a and then from the dielectric half-space) with direction $\varphi_{RDRA} = \pi - \varphi_{ra} = 0.35\pi$ (where $\varphi_{ra} = 2\Phi_a - \varphi_o$) and the double reflected wave (first from the dielectric half-space and then from the face a) with direction $\varphi_{RARD} = 2\Phi_a - \varphi_{rd} = 0.15\pi$ (where $\varphi_{rd} = \pi - \varphi_o$). In region 2 the GO field is composed of the directly transmitted wave through the dielectric half-space with direction $\varphi_{TD} = -\arccos(-\frac{1}{\sqrt{\varepsilon_r}}\cos(\varphi_o)) = -2\pi/3$ and the transmitted wave from the reflected wave of face a with direction $\varphi_{TDRA} = -\arccos(-\frac{1}{\sqrt{\varepsilon_r}}\cos(\varphi_{ra})) \simeq -0.395\pi$. As stated in test case 2, while making classical GO considerations, we need to take into account the different paths of the rays and the local reference system.

The convergence of the solution is obtained for $[A_a, h_a, A_b, h_b] = [10, 0.2, 40, 0.1]$ (see Section III.C). This selection comes from the study of the bands of the kernels in w plane and in particular from our experience in the convergence as done in test case 2.

According to the physical parameters of the problem, we note that the source in the system of FIEs (52) and (53) is only composed of the terms in (50), (51), (31) that contains $u_a(\varphi_o)$ and that does not contains other step functions.

Since Φ_a and Φ_b are acute we need to pay particular attention to the value of γ for the recursive formulas (80)-(83). In this case, we select $\gamma = 1.35$ since $\frac{\pi}{\Phi_a+\Phi_b} \simeq 1.1765$ and $\frac{\pi}{\Phi_a-\Phi_b} \simeq 20$, see Appendix A for details.

Fig. 15 reports the numerical estimations of the GTD coefficient for different values of ε_r from $\varepsilon_r = 1$ to $\varepsilon_r = 10$ (from low dielectric contrast to high dielectric contrast). Note that as expected the GTD coefficient is in region 2 with peaks that converges to $-\pi/2$ for ingreasing values of ε_r. In region 3 we note an interesting and at first sight unexpected behavior of the GTD coefficient: first, for decreasing values of ε_r down to $\varepsilon_r \simeq 1.85$ the GTD decreases since the dominant field in region 3 is a component derived from the reflected field from the dielectric half-space; second, for decreasing values of ε_r from 1.85 to 1 (no layer) we have an increasing values of the GTD field since the dominant field in region 3 is now a component derived from the diffraction by the wedge. As already noted in Fig. 11, Fig. 15 shows a loss of precision for $\varphi_{+k,-k}$ (76). Moreover we note that the GTD coefficient for $\varepsilon_r = 1.001$ is pretty similar to the one exactly obtained for free space case $\varepsilon_r = 1$, except locally at $\varphi_{+k,-k}$ that in this case correspond to the dielectric interface.

Fig. 16 reports the numerical estimations of the total far field at the distance $k_r\rho = 10$ from the edge of the wedge for different values of ε_r from $\varepsilon_r = 1$ to $\varepsilon_r = 10$.

VI. Conclusion

In this paper we present a new method to study the diffraction by PEC wedge over a dielectric half-space at a distance d in the spectral domain. The problem is formulated in a unique entire model based on GWHEs that takes into consideration the true near-field interaction of the wedge with the dielectric

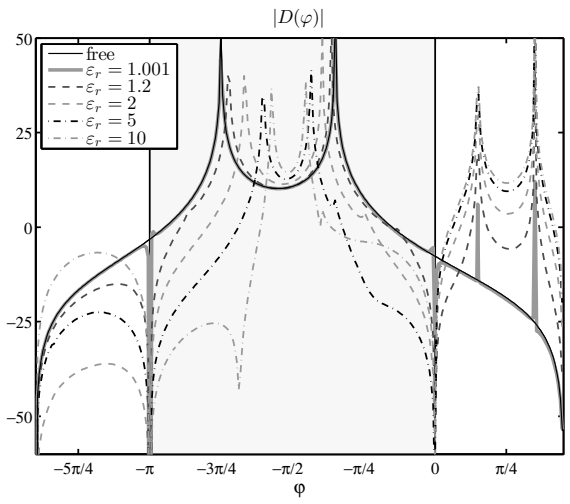

Fig. 15. Test case 3: the absolute value of the GTD diffraction coefficient versus ε_r.

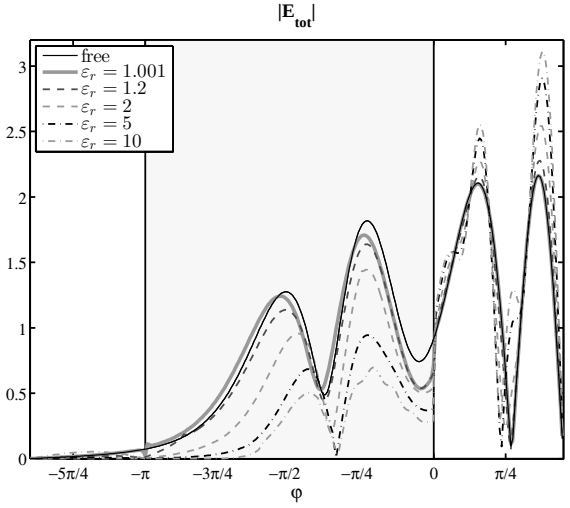

Fig. 16. Test case 3: the total far-field pattern at $k_r\rho = 10$ versus ε_r.

half-space to obtain precise field estimation. In particular the Wiener-Hopf technique is extended to simultaneously deal with problems where angular regions and rectangular regions coexist. The solution is presented in terms of GTD diffraction coefficients, UTD field components and total far fields, with possible applications in radar technologies, antenna development or electromagnetic compatibility.

Appendix A
Analytical Extension

Since the numerical approximation of (52) and (53) yields approximate representations of the axial spectra that are valid in limited strips of the w-plane, we resort to difference equations (recursive equations) to analytically extend the approximate solution. Starting from the system of GWHEs (5), (6), (12), (13), we apply the mapping (17) yielding (20), (32) from (5), (6) and for (12), (13) we obtain

$$\frac{\hat{Y}(w)\hat{V}_d(w)}{\sin w} + \frac{\hat{Y}(w)\hat{V}_{d+}(w+\pi)}{\sin(w+\pi)} + \hat{I}_+(w) - \hat{I}_{\pi+}(w+\pi) = 0 \quad (78)$$

$$\frac{\hat{Y}(-w-\pi)\hat{V}_d(w+\pi)}{\sin(w+\pi)} + \frac{\hat{Y}(-w-\pi)\hat{V}_{\pi d}(w)}{\sin w} + \hat{I}_+(w+\pi) - \hat{I}_{\pi+}(w) = 0 \quad (79)$$

$$\begin{cases} \hat{V}_d(w) = -\dfrac{Z_o\hat{I}_+(2\Phi_a+w) - Z_o\hat{I}_{\pi+}(w+\pi) - \hat{V}_d(2\Phi_a+w) - Z_o\hat{V}_{\pi d}(w+\pi)\hat{Y}(w)\csc(w)}{Z_o\hat{Y}(w)\csc(w)-1} & (80) \\ \hat{I}_+(w) = -\dfrac{Z_o\hat{Y}(w)\hat{I}_+(2\Phi_a+w) + \hat{I}_{\pi+}(w+\pi)\sin(w) + \hat{Y}(w)\hat{V}_d(2\Phi_a+w) + \hat{V}_{\pi d}(w+\pi)\hat{Y}(w)}{Z_o\hat{Y}(w)-\sin(w)} & (81) \\ \hat{V}_{\pi d}(w) = -\dfrac{Z_o\hat{I}_+(w+\pi) - Z_o\hat{I}_{\pi+}(2\Phi_b+w) - Z_o\hat{V}_d(w+\pi)\hat{Y}(-w-\pi)\csc(w) - \hat{V}_{\pi d}(2\Phi_b+w)}{Z_o\hat{Y}(-w-\pi)\csc(w)-1} & (82) \\ \hat{I}_{\pi+}(w) = -\dfrac{\hat{I}_+(w+\pi)\sin(w) - Z_o\hat{Y}(-w-\pi)\hat{I}_{\pi+}(2\Phi_b+w) - \hat{V}_d(w+\pi)\hat{Y}(-w-\pi) - \hat{Y}(-w-\pi)\hat{V}_{\pi d}(2\Phi_b+w)}{Z_o\hat{Y}(-w-\pi)-\sin(w)} & (83) \end{cases}$$

We recall that (20), (32), (78) and (79) are obtained by using the symmetry of functions in w plane. This system of difference equations constitute a different formulation of the problem that can be used to obtain a solution. However difference equations with w-variable coefficients are very cumbersome to treat.

In order to analytically extend the approximate axial spectra, (20), (32), (78) and (79) can be written in the normal form (80)-(83) using mathematical manipulations.

Analytical extensions of $\hat{V}_d(w)$ and $\hat{I}_+(w)$ are obtained via:

$$\hat{V}_d(w) = \begin{cases} \hat{V}_d^{(num)}(w) & -\gamma\,\Phi_a \le \mathrm{Re}[w] \le 0 \\ -\hat{V}_d(-w) & \mathrm{Re}[w] > 0 \\ eq.(80) & \mathrm{Re}[w] < -\gamma\,\Phi_a \end{cases} \quad (84)$$

$$\hat{I}_+(w) = \begin{cases} \hat{I}_+^{(num)}(w) & -\gamma\,\Phi_a \le \mathrm{Re}[w] \le 0 \\ \hat{I}_+(-w) & \mathrm{Re}[w] > 0 \\ eq.(82) & \mathrm{Re}[w] < -\gamma\,\Phi_a \end{cases} \quad (85)$$

where

$$\frac{\pi}{\Phi_a+\Phi_b} < \gamma < Min\left[\frac{\pi}{\Phi_a-\Phi_b}, \frac{3}{2}\right] \quad (86)$$

with $\Phi_a > \Phi_b$. Similar expressions hold for $\hat{V}_{\pi d}(w)$ and $\hat{I}_{\pi+}(w)$ replacing Φ_a with Φ_b, (80) with (82) in (84) and, (81) with (83) in (85). The parameter γ is related to:

- the discretization process yields spurious poles at $Re[w_a], Re[w_b] = -\frac{3\pi}{2}$, respectively for $\hat{V}_d(w), \hat{I}_+(w)$ and $\hat{V}_{\pi d}(w), \hat{I}_{\pi+}(w)$ (see Section III.C),
- the recursive equations (80)-(83) must point to approximate spectra in $-\gamma\Phi_a < w < -\gamma\Phi_a$ for $\hat{V}_d(w)$,$\hat{I}_+(w)$ and in $-\gamma\Phi_b < w < -\gamma\Phi_b$ for $\hat{V}_{\pi d}(w)$ and $\hat{I}_{\pi+}(w)$.

The selection of γ is a trade off: taking the lower bound we obtain good precision since the spectra is far way from the spurious poles, however this choice is less efficient in terms of recursions.

REFERENCES

[1] F. Bertoncini, R. G. Kouyoumjian, G. Manara, and P. Nepa, "High frequency scattering by objects buried in a lossy media," *IEEE Trans. Antennas Propag.,* vol. 49, no. 12, pp. 16491656, Dec. 2001.

[2] F. Bertoncini, G. Manara, P. Nepa and R.G. Kouyoumjian, "EM scattering by a wedge buried in a lossy medium: a UTD solution for the field in the lossy half-space," in Proceedings of the 2004 URSI Electromagnetic Theory Symposium, Pisa, May 23-27, 2004, vol. 2, pp. 1035-1037.

[3] B.A. Baertlein, J.R. Wait, and D.G. Dudley, "Scattering by a conducting strip over a lossy half-space," *Radio Sci.,* vol. 24, no. 4, pp. 485-497, July-Aug. 1989.

[4] A. Imran, Q.A. Naqvi, K. Hongo, "Diffraction of electromagnetic plane wave by an infinitely long conducting strip on dielectric slab," *Opt Comm*, vol. 282, pp. 443-450, 2009

[5] H. Anastassiu, "A closed form physical optics expression for the radar cross section of a perfectly conducting plate over a dielectric halfspace," *Radio Sci.,* vol. 38, no. 2, 1027, pp. 1-13, Apr. 2003.

[6] C.M. Butler, X. Xiao-Bang, and A. Glisson, "Current induced on a conducting cylinder located near the planar interface between two semiinfinite half spaces," *IEEE Trans. Antennas Propag.,* vol. AP-33, no. 6, pp. 616-624, Jun. 1985.

[7] K. A. Michalski and J. R. Mosig, "Multilayered media Greens functions in integral equation formulations," *IEEE Trans. Antennas Propagat.,* vol. 45, pp. 508-519, Mar. 1997

[8] T. J. Cui and W. C. Chew, "Fast evaluation of Sommerfeld integrals for EM scattering and radiation by three-dimensional buried objects," *IEEE Trans. Geosci. Remote Sens.,* vol. 37, no. 2, pp. 887-900, Mar. 1999

[9] N. Geng, A. Sullivan, and L. Carin, "Multilevel fast-multipole algorithm for scattering from conducting targets above or embedded in a lossy half space," *IEEE Trans. Geosci. Remote Sens.,* vol. 38, no. 4, pp. 1551-1560, Jul. 2000.

[10] P. Pawliuk, M. Yedlin, "Multiple Scattering Between Cylinders in Two Dielectric Half-Spaces,"*IEEE Trans. Antennas Propag.,* vol.61, no.8, pp. 4220-4228, Aug. 2013.

[11] R. D. Graglia and G. Lombardi, "Singular higher order complete vector bases for finite methods," *IEEE Trans. Antennas Propag.,* vol. 52, no. 7, pp. 1672-1685, Jul. 2004.

[12] R. D. Graglia and G. Lombardi, "Singular higher order divergenceconforming bases of additive kind and moments method applications to 3D sharp-wedge structures," *IEEE Trans. Antennas Propag.,* vol. 56, no. 12, pp. 3768-3788, Dec. 2008.

[13] V.G. Daniele, "New analytical Methods for wedge problems," in Proceedings of 2001 International Conference on Electromagnetics in Advanced Applications (ICEAA01), Torino, Italy, Sept. 2001, pp. 385-393.

[14] V. Daniele, "The Wiener-Hopf technique for impenetrable wedges having arbitrary aperture angle," *SIAM Journal of Applied Mathematics,* vol.63, n.4, pp.1442-1460, 2003.

[15] V. Daniele, *An introduction to the Wiener-Hopf Technique for the solution of electromagnetic problems,* Internal Report ELT-2004-1, Dipartimento di Elettronica, Politecnico di Torino, Sep. 2004, http://personal.delen.polito.it/vito.daniele/.

[16] V. Daniele, *The Wiener-Hopf technique for wedge problems Dipartimento di Elettronica,* Internal Report ELT-2004-2, Dipartimento di Elettronica, Politecnico di Torino, Oct. 2004, http://personal.delen.polito.it/vito.daniele/.

[17] V.G. Daniele and G. Lombardi, "The Wiener-Hopf technique for impenetrable wedge problems," in Proc. of Days on Diffraction Internat. Conf., invited paper, pp. 50-61, Saint Petersburg, Russia, June 2005, doi: 10.1109/DD.2005.204879.

[18] V. Daniele, and G. Lombardi, "Wiener-Hopf Solution for Impenetrable Wedges at Skew Incidence," *IEEE Trans. Antennas Propagat.,* vol. 54, n. 9, pp. 2472-2485, Sept. 2006.

[19] V. Daniele, "The Wiener-Hopf formulation of the dielectric wedge problem: Part I," Electromagnetics, vol. 30, n. 8, pp. 625-643, 2010.

[20] V. Daniele, "The Wiener-Hopf formulation of the dielectric wedge problem: Part II," Electromagnetics, vol. 31, n. 1, pp. 1-17, 2011.

[21] V. Daniele, "The Wiener-Hopf formulation of the dielectric wedge problem. Part III: The skew incidence case," Electromagnetics, vol. 31, n. 8, pp. 550-570, 2011.

[22] V. Daniele, and G. Lombardi, "The Wiener-Hopf Solution of the Isotropic Penetrable Wedge Problem: Diffraction and Total Field," *IEEE Trans. Antennas Propagat.,* vol. 59, n. 10, pp. 3797-3818, Oct. 2011.

[23] G. Lombardi, "Skew Incidence on Concave Wedge With Anisotropic Surface Impedance," *IEEE Antennas and Wireless Propagation Letters,* vol. 11, pp. 1141-1145, 2012

[24] V.G. Daniele, and G. Lombardi, "Fredholm Factorization for Wedge Problems," Antennas and Propagation Society International Symposium 2006, IEEE, pp. 2478-2481, 9-14 July 2006, Albuquerque, NM, USA, doi: 10.1109/APS.2006.1711100

[25] V.G. Daniele, and G. Lombardi, "Fredholm Factorization of Wiener-Hopf scalar and matrix kernels," *Radio Science,* vol. 42: RS6S01, 2007, doi:10.1029/2007RS003673.

[26] V. Daniele, R. Zich, *The Wiener-Hopf method in electromagnetics,* Mario Boella series on electromagnetism in information and communication series, Raleigh, NC: SciTech Publishing, 2014

[27] L. B. Felsen and N. Marcuvitz, *Radiation and Scattering of Waves,* Englewood Cliffs, NJ: Prentice-Hall, 1973.

[28] B. Budaev, *Diffraction by wedges,* London, UK: Longman Scient., 1995.

[29] T.B.A. Senior, and J.L. Volakis, *Approximate boundary conditions in electromagnetics,* London, UK: IEE, 1995.

[30] J. M. L. Bernard, "Diffraction at skew incidence by an anisotropic impedance wedge in electromagnetism theory: A new class of canonical cases," *J. Physics A: Math. Gen.,* vol. 31, no. 2, pp. 595-613, 1998.

[31] V.M. Babich, M.A. Lyalinov, and V.E. Grikurov, *Sommerfeld-Malyuzhinets Technique in Diffraction Theory,* Oxford, UK: Alpha Science, 2007.

[32] A.V. Osipov, "On the method of Kontorovich-Lebedev integrals in problems of wave diffraction in sectorial media," in *Problems of diffraction and propagation of waves*, Vol. 25, pp. 173-219, St Petersburg University Publications, 1993.

[33] A.D. Rawlins, "Diffraction by, or diffusion into, a penetrable wedge," *Proc. Royal Society Math., Phys. Engrng. Sci.,* 455, pp.2655-2686, 1999.

[34] M.A. Salem, A. Kamel, and A.V. Osipov, "Electromagnetic fields in the presence of an infinite dielectric wedge," *Proc. Royal Society Math., Phys. Engrng. Sci.,* vol. 462, pp. 2503-2522, 2006.

[35] V.G. Daniele, *Electromagnetic fields for PEC wedge over stratified media,* Internal Report ELT-2013-1, DET, Politecnico di Torino, 2013, http://personal.delen.polito.it/vito.daniele/.

[36] V.G. Daniele, "Electromagnetic fields for PEC wedge over stratified media. Part I," *Electromagnetics*, vol. 33, pp. 179-200, 2013.

[37] V.G. Daniele, and G. Lombardi, "Wiener-Hopf Formulation of an Unaligned PEC Wedge over a Stratification," Proc. 2015 IEEE Antennas and Propagation Society Int. Symp., pp.185-186.

[38] V.G. Daniele, and G. Lombardi, "Wiener-Hopf Solution for an Unaligned PEC Wedge over a Dielectric Substrate," Proc. 2015 International Conference on Electromagnetics in Advanced Applications (ICEAA15), Torino, Italy, pp.1530-1533, 7-11 Sept. 2015

[39] V.G. Daniele, "Rotating Waves in the Laplace Domain for Angular Regions," *Electromagnetics,*, vol. 23, n. 3, pp. 223-236, 2003.

[40] L.V. Kantorovich and V.I. Krylov, *Approximate methods of higher analysis,* Groningen, The Netherlands: Noordhoff, 1964.

[41] R. G. Kouyoumjian and P. H. Pathak, "A uniform geometrical theory of diffraction for an edge in a perfectly conducting surface," *Proc. IEEE,* vol. 62, pp. 1448-1461, Nov. 1974.

Vito Daniele was born in Catanzaro, Italy, on March 20, 1942. He received the degree in electronic engineering from Polytechnic of Turin, Italy, in 1966. In 1980, he was appointed Full Professor in Electrical Engineering at the University of Catania.

From 1981 to 2012 he was Professor of Electrical Engineering at the Polytechnic of Turin and since 2015 he is Emeritus Professor at the same Polytechnic. He has served also as a Consultant to various industries in Italy. He has published more than 150 papers in refereed journals and conference proceedings and several textbook chapters.

His research interests are mainly in analytical and approximate techniques for the evaluation of electromagnetic fields both in high and in low frequency. In particular his studies on the Wiener Hopf technique have produced the recent book "The Wiener-Hopf Method in Electromagnetics". Prof. Daniele was the Guest Editor of a special issue on Electromagnetic Coupling to Transmission Lines for Electromagnetics in 1988, Chairman and Invited Speaker for several international symposia, and reviewer for many international journals.

Since 2013 he is corresponding Member of the Academy of Sciences of Torino.

Guido Lombardi (S'02-M'03-SM'11-) was born in Florence, Italy, on December 8, 1974. He received the Laurea degree (*summa cum laude*) in telecommunications engineering from the University of Florence, Italy, in 1999 and the Ph.D. degree in electronics engineering at the Polytechnic of Turin, Italy, in jan. 2004. In 2000-01, he was officer of the Italian Air Force. In 2004 he was an Associate Researcher with the Department of Electronics of Polytechnic of Turin and in 2005 he joined the same Department as an Assistant Professor with tenure and where he is currently an Associate Professor. He was the recipient of the Raj Mittra Travel Grant award for junior researcher at 2003 IEEE AP-S International Symposium and USNC/CNC/URSI National Radio Science Meeting, Columbus, OH, USA. In the same year he was Visiting Researcher at the Department of Electrical and Computer Engineering, University of Houston, Houston, TX, USA.

His research interests comprise analytical and numerical methods for electromagnetics, Wiener-Hopf method, diffraction, theoretical and computational aspects of FEM and MoM, numerical integration, electromagnetic singularities, waveguide problems, microwave passive components, project of orthomode transducers (OMT), metamaterials.

He is an associate editor of the IEEE ACCESS journal an IEEE APS AdCom member for the triennium (2016-18). He served as member of the Organizing Committee in the International Conference on Electromagnetics in Advanced Applications (ICEAA) since the 2001 edition and in the IEEE-APS Topical Conference on Antennas and Propagation in Wireless Communications (IEEE-APWC) since the 2011 edition. He was Publication Chair of ICEAA and IEEE-APWC in 2011, 2013-2014 editions. He served the 2012 IEEE AP-S International Symposium and USNC/CNC/URSI National Radio Science Meeting, Chicago, IL, USA as co-organizer of the Special Session entitled "Challenging Canonical Scattering Problems and New EM Problems involving Special Materials".

He regularly serves as a reviewer of several international journals on physics, electrical engineering and electromagnetics, among which IEEE, IET, Wiley, Elsevier, PLoS, ACES Journals and Transactions.